Available online at www.sciencedirect.com
SCIENCE DIRECT®
Journal of Sound and Vibration 290 (2006) 65–100
JOURNAL OF SOUND AND VIBRATION
www.elsevier.com/locate/jsvi

Nonlinear dynamic analysis of a high-speed rotor supported by rolling element bearings

S.P. Harsha*

Mechanical Engineering Group, Birla Institute of Technology & Science, Pilani 333031, India

Received 26 January 2004; received in revised form 4 March 2005; accepted 14 March 2005
Available online 31 May 2005

Abstract

The paper presents an analytical model for investigating structural vibrations of a high-speed rotor supported by rolling bearings. The mathematical formulation accounted for tangential motions of rolling elements as well as inner and outer races with the sources of nonlinearity such as Hertzian contact force, geometrical imperfections, i.e. surface waviness and radial internal clearance, resulting transition from no-contact to contact state between rolling elements and the races. In the formulation the contacts between the rolling elements and the races are considered as nonlinear springs, whose stiffnesses are obtained by using Hertzian elastic contact deformation theory. The implicit type numerical integration technique Newmark-β with Newton–Raphson method is used to solve the nonlinear differential equations iteratively. The results show the appearance of instability and chaos in the dynamic response as the speed of the rotor-bearing system is changed. Period doubling and mechanism of intermittency have been observed as the routes to chaos. The appearance of regions of periodic, sub-harmonic and chaotic behavior is seen to be strongly dependent on rotor speed and these imperfections. Poincarè maps and frequency spectra are used to elucidate and to illustrate the diversity of the system behavior.

1. Introduction

The vibration analysis of the rotor-bearing system is becoming more important as demands on running accuracy are increased. Growing interest is devoted to rolling bearings, not only as

*Tel.: +91 01596 242210; fax: +91 01596 244183.
E-mail address: spharsha@yahoo.com.

0022-460X/$ - see front matter © 2005 Elsevier Ltd. All rights reserved.
doi:10.1016/j.jsv.2005.03.008

Nomenclature

$F_u =$ unbalance rotor force, N
$I =$ moment of inertia of each rolling element
$I_{\text{rotor}} =$ moment of inertia of the rotor
$I_{\text{in}} =$ moment of inertia of the inner race
$I_{\text{out}} =$ moment of inertia of the outer race
$K_{\text{in}} =$ nonlinear stiffness of the inner race
$K_{\text{out}} =$ nonlinear stiffness of the outer race
$L =$ arc length, mm
$m_{\text{in}} =$ mass of the inner race, kg
$m_j =$ mass of the rolling elements, kg
$m_{\text{out}} =$ mass of the outer race, kg
$m_{\text{rotor}} =$ mass of the rotor, kg
$N_w =$ number of wave lobes
$N_b =$ number of rollers
$R =$ radius of the outer race
$r =$ radius of the inner race
$r_{\text{in}} =$ position of mass center of the inner race
$r_{\text{out}} =$ position of mass center of the outer race
$T =$ kinetic energy of the bearing system
$T_{\text{rotor}} =$ kinetic energy of the rotor
$T_{\text{i\_race}} =$ kinetic energy of the inner race
$T_{\text{o\_race}} =$ kinetic energy of the outer race
$T_{\text{r.e.}} =$ kinetic energy of the rolling elements
$V =$ potential energy of the bearing system
$V_{\text{rotor}} =$ potential energy of the rotor
$V_{\text{i\_race}} =$ potential energy of the inner race
$V_{\text{o\_race}} =$ potential energy of the outer race
$V_{\text{r.e.}} =$ potential energy of the rolling elements
$V_{\text{springs}} =$ potential energy of the springs
$x_{\text{in}}, y_{\text{in}} =$ center of the inner race
$x_{\text{out}}, y_{\text{out}} =$ center of the outer race
$\delta_{\text{in}} =$ deformation at the point of contact at the inner race
$\delta_{\text{out}} =$ deformation at the point of contact at the outer race
$(\dot{\phi})_{\text{in}} =$ angular velocity of the inner race
$(\dot{\phi})_{\text{out}} =$ angular velocity of the outer race
$\gamma_0 =$ internal radial clearance, μm
$\lambda =$ wavelength, mm
$\omega_{\text{cage}} =$ angular velocity of cage relating to the cage
$(\Pi)_0 =$ initial amplitude of the wave at race, μm
$(\Pi)_p =$ maximum amplitude of the wave at race, μm
$\rho_j =$ radial position of the rolling element
$\rho_r =$ radius of each rolling element
$\theta_j =$ angular position of rolling element
$\chi_j =$ position of jth rolling element from the center of the inner race
VC = varying compliance frequency

structural elements but also as sources of vibration. In general, the rotor-bearing system displays nonlinear behavior due to nonlinear Hertzian contact force, bearing clearances, and surface waviness with high-speed rotor. The behavior of the nonlinear system often demonstrates unexpected behavior patterns that are extremely sensitive to initial conditions. The most fundamental cause of rolling bearing vibration is the periodic variation of assembly stiffness that arises as the cage rotates. There is also a parametric effect because of the varying compliance (VC) of the bearing. This study is restricted to roller bearings with a pure radial load. In practice such bearings will normally have a small positive clearance, either present already when the bearing is fitted or gradually developing with wear. The approach used in this paper presupposes the existence of such a clearance.

Clearance, which is provided in the design of bearing to compensate the thermal expansion, is also a source of vibration and introduces the nonlinearity in the dynamic behavior. The study of the effect of clearance nonlinearity on the response of rotors has gained a lot of attention lately because of the development of high-speed rotors such as the space shuttle main engine turbo-pump rotor. Clearance nonlinearity is different from most of other nonlinearities because it cannot be approximated by a mathematical series. The early work in rotor dynamics by

Yamamoto [1] introduces nonlinearity to the Jeffcott equation by including the effect of bearing clearances (or dead bands). The conclusion of this work shows that the maximum amplitude at critical speed decreases with increasing radial clearance and critical speed disappears under the condition beyond a marginal clearance, which depends on the amount of unbalance. The VC effect was studied theoretically by Perret [2] considering a deep groove ball bearing with the elastic deformation between race and balls modeled by the Hertzian theory and no bending of races. Meldau [3] theoretically studied the 2D motion of shaft center. Both Perret [2] and Meldau [3] performed a quasi-static analysis since inertia and damping force were not taken into account.

Sunnersjo [4] studied the VC vibrations theoretically and experimentally, taking inertia and damping forces into account. Fukata et al. [5] first took up the study of VC vibrations and the nonlinear dynamic response for the ball bearing supporting a balanced horizontal rotor with a constant vertical force. It is a more detailed analysis as compared to Sunnersjo's [4] work as regimes of super-harmonic, sub-harmonic and chaotic behavior are found out. Mevel and Guyader [6] have developed a theoretical model of a ball bearing supporting a balanced horizontal rigid rotor, with a constant vertical radial force. This is similar to the work done by Fukata et al. [5] but more results have been reported for parametric studies undertaken and routes to chaos traced out. Chaos in this model of bearing has been reported to come out of the sub-harmonic route and the quasi-periodic route.

The arc length continuation technique has been used for obtaining dynamic characteristics of ball bearings by Sankaravelu et al. [7]. This technique enables one to identify the possible parameter ranges for which the jump phenomena or the sudden change of the dynamic behavior of the system occurs. The ball bearing taken for study supports a constant vertical radial load of a balanced horizontal rotor. Sankaravelu et al. [7] have reported that the arc length continuation method takes less computation time when compared to direct integration, and the method obtains steady-state response and stability analysis simultaneously. The eigenvalues of the Floquet matrix are obtained with the shooting technique, which gives the bifurcation points. The system Sankaravelu et al. [7] have taken for study is the same as that taken by Fukata et al. [5]. This work reports the appearance of chaotic response due to the intermittency. Once the stability sets in numerical integration, it is used to obtain the response. Tamura et al. [8] have theoretically estimated the stiffness of the ball bearing subjected to a constant radial load. Gargiulo [9] has developed a new set of equations for providing initial estimates of stiffness of rolling element bearings.

Yamauchi [10] developed a numerical harmonic balance method using the FFT algorithm for multiple degree of freedom rotor systems, including nonlinear bearings and couplings. Saito [11] calculated the nonlinear unbalance response of horizontal Jeffcott rotors with radial clearance. Both studies were concerned only with the harmonic response. Childs [12] presented an explanation for the sub-harmonic response of rotors in the presence of bearing clearance and side load. Choi and Noah [13] analyzed the coherence of super- and sub-harmonic in a rotor-bearing model using the harmonic balancing method along with a discrete Fourier transform procedure. For multi-disk rotor systems, Nataraj and Nelson [14] developed a periodic solution method based on a collocation approach for the response of the rotor. They utilized a sub-system approach to reduce the size of the resulting system of algebraic equations. The dynamic responses of rotors in high-speed rotors with bearing clearance have been studied by Ehrich [15–17]. These studies by Ehrich show the appearance of high sub-harmonic and chaotic response in the rotor.

Apart from super- and sub-harmonic responses, aperiodic whirling motions in a high-pressure oxygen turbo pump of the space shuttle main were also reported by Kim and Noah [18].

It is generally accepted that it is not possible to produce a perfect surface or contour even with the best machine tools and this also applies to ball-bearing manufacturing. Surface waviness is a manufacturing imperfection. An imperfection is called waviness if its wavelength is much longer than the Hertzian contact width. It may be caused by different manufacturing malfunctions such as uneven wear of the wheel in grinding operations, variable interactions between the tool and work piece, vibrations of machine elements or movements of the work in the fixture, etc. Choudhury and Tandon [19] presented a theoretical model to obtain vibration response by considering distributed defects as waviness at the races and off-size rolling elements. Meyer et al. [20] presented a mathematical technique to predict the spectral components of vibrations emanating from the effects like misaligned races, eccentric races, off size rolling elements and outer race waviness. Expressions were derived for radial displacement of the bearing stationary race. Wardle and Poon [21] also pointed out the relation between the number of balls and waves for severe vibrations to occur. When the number of balls and waves are equal there will be severe vibrations. Wardle [22] showed that ball waviness produced vibrations in the axial and radial directions at different frequencies. Aktürk [23] presented a mathematical model consisting of inner, outer and ball waviness and showed that for inner race most vibrations occur when the ball passage frequency and its harmonics coincide with the natural frequency.

In this work, the effects of rotor speed with geometrical imperfections have been studied. The appearance of periodic, sub-harmonic, chaotic and Hopf bifurcation is seen theoretically. The results presented here have been obtained from a large number of numerical integrations and are mainly presented in the form of Poincarè maps and frequency spectra.

2. Problem formulation

In this section, a mathematical model for the analysis of the structural vibration in rolling element bearings has been developed. Initially the expressions for kinetic and potential energies are formulated for all components of rolling element bearing. The equations of motion, which describe the dynamic behavior of the complex model, have been derived by considering these energies expression and the Lagrange's equations. A schematic diagram of rolling element bearing is shown in Fig. 1. For investigating the structural vibration characteristics of rolling element bearing, a model of bearing assembly can be considered as a spring–mass system, in which the outer race of the bearing is fixed in a rigid support and the inner race is fixed rigidly with the rotor. A constant radial force acts on the system.

In the mathematical modeling, the rolling element bearing is considered as the spring–mass system and rolling elements act as nonlinear contact spring as shown in Fig. 2. Since the Hertzian forces arise only when there is contact deformation, the springs are required to act only in compression. In other words, the respective spring force comes into play when the instantaneous spring length is shorter then its unstressed length, otherwise the separation between the rolling element and the races takes place and the resultant force is set to zero. A real rotor-bearing system is generally very complicated and difficult to model; so, for an effective and simplified

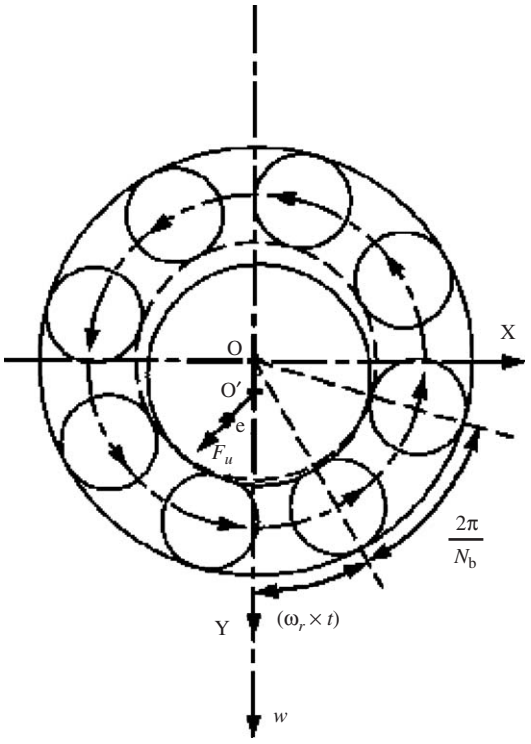

Fig. 1. A schematic diagram of a rolling bearing.

mathematical model the following assumptions are made:

1. Deformations occur according to the Hertzian theory of elasticity. Small elastic deformations of the rolling elements and the races are considered but plastic deformations are neglected.
2. The rolling elements, the inner and outer races and the rotor have motions in the plane of bearing only.
3. The angular velocity of the cage is assumed to be constant.
4. The rollers in a rolling element bearing are assumed to have no angular rotation about their axes, i.e. no skewing. Hence, there is no interaction of the corners of the rollers with the cage and the flanges of the races.
5. All the bearing components and the rotor are rigid, i.e. there is no bending.
6. The bearings are assumed to operate under isothermal conditions. Hence, all thermal effects that may arise due to the rise in temperature, such as change of lubricant viscosity, expansion of the rolling elements and the races and reduction of endurance of the material, are considered absent.
7. There is no slipping of rollers as they roll on the surface of races. Since there is perfect rolling of the rollers on the surface of races and the two points of rollers touching the races have different linear velocities, the center of the roller has a resultant translational velocity.
8. The damping of a roller bearing is very small. This damping is present because of friction and a small amount of lubrication. The estimation of the damping of roller bearing is very difficult because of the dominant extraneous damping which swamps the damping of the bearing.

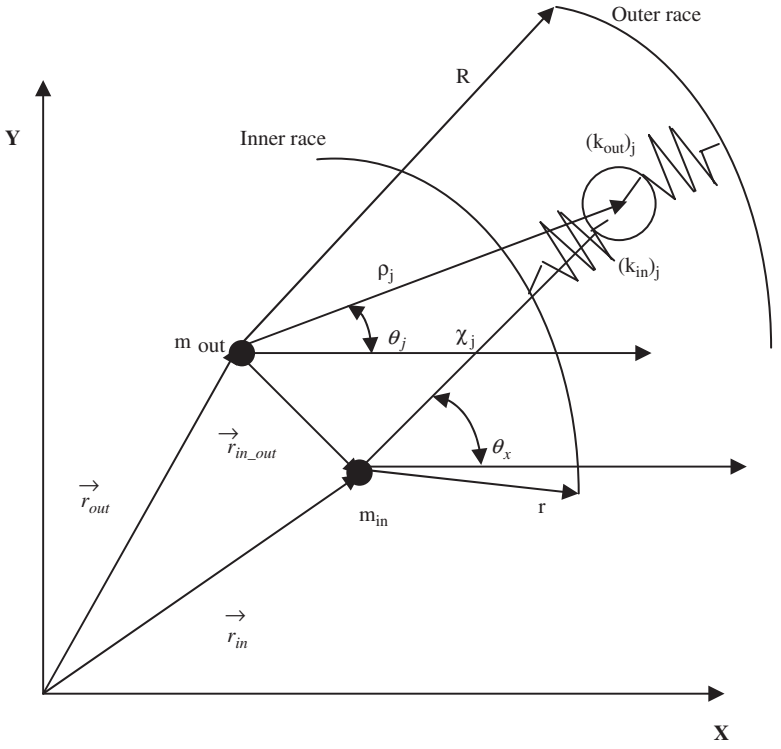

Fig. 2. Mass–spring model of the rolling bearing.

9. The cage ensures the constant angular separation (β) between rolling elements, hence, there is no interaction between rolling elements. In addition, at any given instant, some of the rolling elements will contact both races. Hence,

$$\beta = \frac{2\pi}{N_b}. \tag{1}$$

2.1. Race waviness

An important source of vibrations in rolling bearings is waviness. These are global sinusoidal-shaped imperfections on the outer surface of the bearing components. Waviness is realized in the form of peaks and valleys of varying height and width. Therefore, for mathematical modeling using the waviness effect, a statistical approach is necessary in order to have a complete solution. If the races are assumed to bend due to rolling element loads, then the flexural vibrations of the races as well as the rigid body motion have to be considered. To avoid these problems the races are assumed bendless under these loads and a sinusoidal wavy surface is assumed as shown in Fig. 3(a). The wavelength is assumed to be much longer than the roller-to-race foot print width and the wave geometry itself is assumed to be unaffected by contact distortion. Waves are described in terms of two parameters: the wavelength (λ), which is the distance taken by a single cycle of the wave and its amplitude (Π_i).

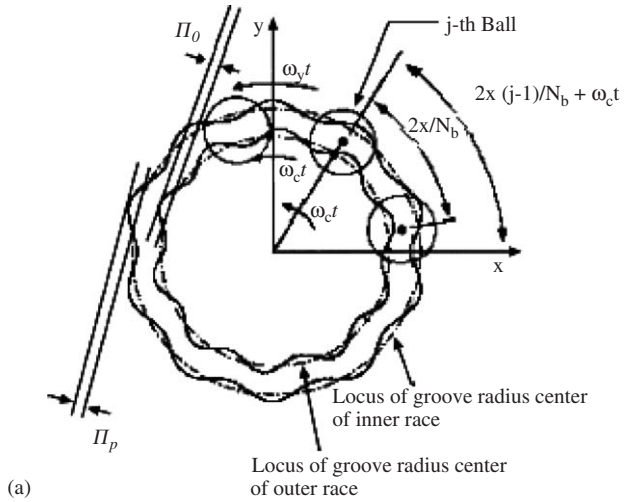

(a)

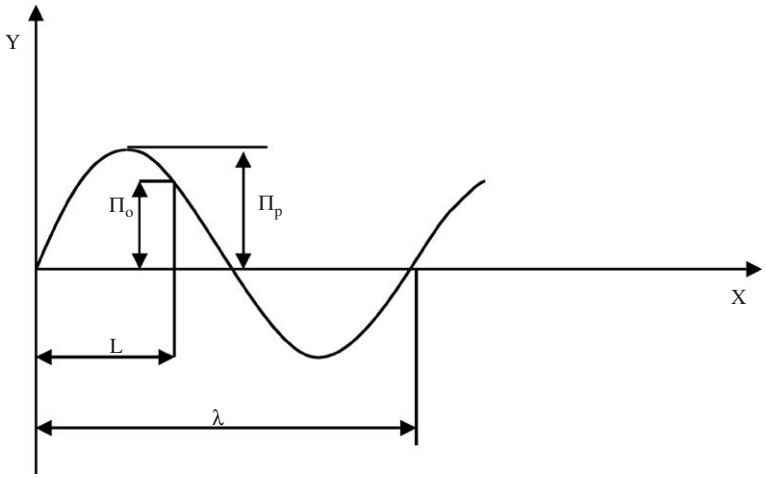

(b)

Fig. 3. (a) Race waviness model; (b) wave of the race.

The amplitude of the wavy surface is often measured with respect to the central point at a certain angle from the reference axis. Hence, the amplitude of the sinusoidal wave is

$$(\Pi)_i = \Pi_p \sin\left(2\pi \frac{L}{\lambda}\right). \tag{2}$$

The race circumference has a sinusoidal wavy surface, therefore, the radial clearance consists of a constant part and a variable part. Hence, the amplitude of the wave of race is

$$(\Pi)_i = (\Pi_0) + (\Pi_p) \sin\left(2\pi \frac{L}{\lambda}\right), \tag{3}$$

where Π_p is the maximum amplitude of the wave and Π_0 is the initial wave amplitude (or constant clearance) as shown in Fig. 3(b).

The arc length (L) of the wave at the contact angle is

$$L = r\theta_j. \tag{4}$$

The wavelength is the ratio of the length of the race circumference to the number of waves on circumference, which is

$$\lambda = \frac{2r\pi}{N_w}. \tag{5}$$

The amplitude of the race waves at the contact angle is

$$(\Pi)_i = (\Pi_0) + (\Pi_p)\,\sin(N_w\theta_j). \tag{6}$$

Hence, the contact angle is

$$\theta_j = \frac{2\pi}{N_b}(j-1) + \omega_{\text{cage}} \times t. \tag{7}$$

The cage speed ω_{cage} is

$$\omega_{\text{cage}} = \frac{1}{2}\,\omega_{\text{inner}}\left[1 - \frac{\rho_j}{R_p}\right] + \frac{1}{2}\,\omega_{\text{outer}}\left[1 + \frac{\rho_j}{R_p}\right]. \tag{8}$$

The VC frequency is

$$\omega_{\text{vc}} = N_b\omega_{\text{cage}}. \tag{9}$$

Hence, the instantaneous amplitude of waviness at the contact angle is

$$(\Pi)_i = (\Pi_0) + (\Pi_p)\,\sin\left[N_w\left\{\frac{2\pi}{N_b}(j-1) + \omega_{\text{cage}} \times t\right\}\right]. \tag{10}$$

2.2. Contact stiffness

Hertz considered the stress and deformation in the perfectly smooth, ellipsoidal, contacting elastic solids. The application of the classical theory of elasticity to the problem forms the basis of stress calculation for machine elements as ball and roller bearings. Therefore, the line contact between the race and roller develops into an area contact, which has the shape of an ellipse with a and b as the semi-major and semi-minor axes, respectively. The curvature sum and difference are needed in order to obtain the contact force of the roller. Hertz equations for elastic deformation involving *line* contact between solid bodies are given by Eschmann et al. [24] as

$$\delta = \frac{4.05}{10^5}\,\frac{Q^{0.925}}{l_{\text{eff}}^{0.85}} \quad \text{(mm)}. \tag{11}$$

Here, l_{eff} is the length over which rollers are actually in contact. The contact force is

$$Q = 56065.703 \times l_{\text{eff}}^{0.92}\delta^{1.08} \quad \text{(N)}. \tag{12}$$

Hence, the nonlinear stiffness associated with the *line* contact is given as

$$k = \frac{Q}{\delta} = 56065.703 \times l_{\text{eff}}^{0.92}\delta^{0.08} \quad (\text{N/mm}). \tag{13}$$

2.3. Derivation of governing equations of motion

The equations of motion that describe the dynamic behavior of the complete model can be derived by using Lagrange's equation for a set of independent generalized coordinates as

$$\frac{\mathrm{d}}{\mathrm{d}t}\frac{\partial T}{\partial\{\dot{p}\}} - \frac{\partial T}{\partial\{p\}} + \frac{\partial V}{\partial\{p\}} = \{f\}, \tag{14}$$

where T, V, p and f are kinetic energy, potential energy, vector with generalized degree-of-freedom (dof) coordinate and vector with generalized contact forces, respectively. The kinetic and potential energies can be subdivided into the contributions from the various components, i.e. from the rolling elements, the inner race, the outer race and the rotor.

The total kinetic energy (T) of the rotor-bearing system is the sum of the rolling elements, inner and outer races and the rotor and is written as

$$T = T_{\text{r.e.}} + T_{\text{i\_race}} + T_{\text{o\_race}} + T_{\text{rotor}}. \tag{15}$$

The subscripts i_race, o_race and cage refer to, respectively, the inner race, the outer race and the cage. The subscript r.e. indicates the rolling elements.

The potential energy is provided by deformations of the balls with the races and deformations occur according to Hertzian contact theory of elasticity. Potential energy formulation is performed taking datum as the horizontal plane through the global origin. The total potential energy (V) of the bearing system is the sum of the balls, inner and outer races, springs and the rotor and is written as

$$V = V_{\text{r.e.}} + V_{\text{i\_race}} + V_{\text{o\_race}} + V_{\text{springs}} + V_{\text{rotor}}, \tag{16}$$

where $V_{\text{r.e.}}$, $V_{\text{i\_race}}$, $V_{\text{o\_race}}$ and V_{rotor} are the potential energies due to elevation of the rolling elements, inner and outer races and the rotor, respectively. V_{springs} is the potential energy due to nonlinear spring contacts between rollers and the races.

2.3.1. Contribution of the inner race

Apart from local deformations in the contacts, the inner race is considered as a rigid body. The kinetic energy of the inner race about its center of mass is evaluated in x- and y-frame. The position of the origin of the moving frame relative to the reference frame is described by transitional dof $\dot{x}_{\text{in}}$ and $\dot{y}_{\text{in}}$.

The kinetic energy expression for the inner race is:

$$T_{\text{i\_race}} = \frac{1}{2}m_{\text{in}}(\dot{\vec{r}}_{\text{in}} \cdot \dot{\vec{r}}_{\text{in}}) + \frac{1}{2}I_{\text{in}}\dot{\phi}_{\text{in}}^2. \tag{17}$$

The displacement vector showing the location of the inner race center with respect to that of the outer race center is then given by

$$\vec{r}_{\text{in}} = \vec{r}_{\text{out}} + \vec{r}_{\text{in\_out}} \tag{18}$$

or

$$\vec{r_{\text{in}}} = \left(\vec{x_{\text{in}}} + \vec{x_{\text{out}}}\right)\hat{i} + \left(\vec{y_{\text{in}}} + \vec{y_{\text{out}}}\right)\hat{j}. \tag{19}$$

Differentiating r_{in} with respect to time (t) and putting that value in Eq. (17) gives

$$T_{\text{i\_race}} = \frac{1}{2} m_{\text{in}}(\dot{x}_{\text{in}}^2 + \dot{y}_{\text{in}}^2) + \frac{1}{2} I_{\text{in}}\dot{\phi}_{\text{in}}^2. \tag{20}$$

Since the position of the inner race is defined from the outer race center, the potential energy for the inner race is

$$V_{\text{i\_race}} = m_{\text{in}} g(y_{\text{in\_out}} + y_{\text{out}}). \tag{21}$$

2.3.2. Contribution of the outer race

The outer race is also considered as a rigid body and it is assumed that the outer race is stationary. Hence, $\dot{r}_{\text{out}} = 0$ and $\dot{\phi}_{\text{out}} = 0$.

The kinetic energy expression for the outer race is zero.

The potential energy of the outer race is

$$V_{\text{o\_race}} = m_{\text{out}}\, g y_{\text{out}}. \tag{22}$$

2.3.3. Contribution of the rolling elements

The rolling elements are also considered as rigid bodies. For the determination of their contribution to the kinetic energy, the position of the jth-rolling element is describe by two transitional dof,

$$(\dot{\rho}_j + \dot{r}_{\text{out}}) \quad \text{and} \quad \dot{\phi}_j.$$

The kinetic energy due to rolling elements is to be obtained as a summation of those from each element as

$$T_{\text{r.e.}} = \sum_{j=1}^{N_b} T_j. \tag{23}$$

The position of the center of the roller is defined with respect to the outer race center. Hence, the kinetic energy of the rolling elements may be written as

$$T_j = \frac{1}{2} m_j(\dot{\vec{\rho}}_j + \dot{\vec{r}}_{\text{out}}) \cdot (\dot{\vec{\rho}}_j + \dot{\vec{r}}_{\text{out}}) + \frac{1}{2} I_j \dot{\phi}_j^2. \tag{24}$$

The displacement vector showing the location of jth rolling elements is

$$\vec{\rho}_j = (\rho_j \cos\theta_j)\hat{i} + (\rho_j \sin\theta_j)\hat{j}. \tag{25}$$

For the outer race center it is

$$\vec{r}_{\text{out}} = \vec{x}_{\text{out}}\hat{i} + \vec{y}_{\text{out}}\hat{j}. \tag{26}$$

The summation of Eqs. (25) and (26) after differentiation with respect to time (t) leads to the following expression:

$$\begin{aligned}(\dot{\vec{\rho}}_j + \dot{\vec{r}}_{\text{out}}) \cdot (\dot{\vec{\rho}}_j + \dot{\vec{r}}_{\text{out}}) = {} & \dot{\rho}_j^2 \cos^2\theta_j + \rho_j^2 \sin^2\theta_j \cdot \dot{\theta}_j^2 - 2\dot{\rho}_j \cdot \rho_j \cdot \dot{\theta}_j \cos\theta_j \sin\theta_j \\ & + \dot{x}_{\text{out}}^2 + 2\dot{x}_{\text{out}}(\dot{\rho}_j \cos\theta_j - \rho_j \sin\theta_j \cdot \dot{\theta}_j) + \dot{\rho}_j^2 \sin^2\theta_j \\ & + \rho_j^2 \cos^2\theta_j \cdot \dot{\theta}_j^2 + 2\dot{\rho}_j \cdot \rho_j \cdot \dot{\theta}_j \cos\theta_j \sin\theta_j \\ & + \dot{y}_{\text{out}}^2 + 2\dot{y}_{\text{out}}(\dot{\rho}_j \cos\theta_j - \rho_j \sin\theta_j \cdot \dot{\theta}_j). \end{aligned} \tag{27}$$

The outer race is assumed to be stationary, hence $\dot{x}_{\text{out}} = 0$ and $\dot{y}_{\text{out}} = 0$. Therefore, Eq. (27) becomes

$$(\dot{\vec{\rho}}_j + \dot{\vec{r}}_{\text{out}}) \cdot (\dot{\vec{\rho}}_j + \dot{\vec{r}}_{\text{out}}) = \dot{\rho}_j^2 \cos^2\theta_j + \rho_j^2 \sin^2\theta_j \cdot \dot{\theta}_j^2 + \dot{\rho}_j^2 \sin^2\theta_j + \rho_j^2 \cos\theta_j \cdot \dot{\theta}_j^2 \tag{28}$$

or

$$(\dot{\vec{\rho}}_j + \dot{\vec{r}}_{\text{out}}) \cdot (\dot{\vec{\rho}}_j + \dot{\vec{r}}_{\text{out}}) = (\dot{\rho}_j^2 + \rho_j^2 \cdot \dot{\theta}_j^2). \tag{29}$$

From Eq. (24), we get

$$T_j = \frac{1}{2} m_j(\dot{\rho}_j^2 + \rho_j^2 \cdot \dot{\theta}_j^2) + \frac{1}{2} I_j \dot{\phi}_j^2. \tag{30}$$

It is assumed that there is no slip, hence, the relative transitional velocity of the outer race and rolling element must be same and in opposite direction. Therefore, the contact equation for the jth-rolling element and the outer race can be written as

$$\rho_r(\dot{\phi}_j - \dot{\theta}_j) = -R(\dot{\phi}_{\text{out}} - \dot{\theta}_j). \tag{31}$$

Since the outer race is stationary,

$$\dot{\phi}_{\text{out}} = 0. \tag{32}$$

The rotation of the jth-rolling element about its center of mass is

$$\dot{\phi}_j = \dot{\theta}_j\left(1 + \frac{R}{\rho_r}\right). \tag{33}$$

Now the kinetic energy of the rolling elements can be written as

$$T_{\text{r.e.}} = \sum_{j=1}^{N_b} \frac{1}{2} m_j(\dot{\rho}_j^2 + \rho_j^2 \cdot \dot{\theta}_j^2) + \frac{1}{2} I_j \dot{\theta}_j^2 \left(1 + \frac{R}{\rho_r}\right)^2. \tag{34}$$

The position of the center of the roller is defined with respect to the outer race center. Hence, the potential energy of the rolling elements may be written as

$$V_{\text{r.e.}} = \sum_{j=1}^{N_b} m_j g(\rho_j \sin\theta_j + y_{\text{out}}) \tag{35}$$

or

$$V_{\text{r.e.}} = m\,g\,N_b y_{\text{out}} + \sum_{j=1}^{N_b} (m_j g\,\rho_j \sin\,\theta_j). \tag{36}$$

2.3.4. Contribution of the rotor

The kinetic energy of the rotor is calculated by assuming that its center remains coincident with the inner race. Hence, the kinetic energy of the rotor is

$$T_{\text{rotor}} = \frac{1}{2}\, m_{\text{rotor}}(\dot{x}_{\text{in}}^2 + \dot{y}_{\text{in}}^2) + \frac{1}{2}\, I_{\text{rotor}}\, \dot{\theta}_{\text{rotor}}^2. \tag{37}$$

The rotor center coincides with the inner race center and position of the inner race center is defined with respect to the outer race center. Hence, the potential energy of the rotor is expressed as

$$V_{\text{rotor}} = m_{\text{rotor}} g(y_{\text{in\_out}} + y_{\text{out}}). \tag{38}$$

2.3.5. Contribution of the contact deformation

The contacts between balls and races are treated as nonlinear springs, whose stiffness is obtained by Hertzian theory of elasticity. The expression of potential energy due to the contact deformation of the springs is

$$V_{\text{spring}} = \sum_{j=1}^{N_b} \frac{1}{2}\, k_{\text{in}} \delta_{\text{in}}^2 + \sum_{j=1}^{N_b} \frac{1}{2}\, k_{\text{out}} \delta_{\text{out}}^2. \tag{39}$$

The deformation at contact points between the jth rolling element and the inner race is

$$\delta_{\text{in}} = [\{r + \rho_r\} - \chi_j]. \tag{40}$$

In this expression, if $\{r + \rho_r\} > \chi_j$, compression takes place and restoring force acts.

If $\{r + \rho_r\} < \chi_j$, no compression and restoring force is set equal to zero.

Similarly, at the outer race the deformation at the contact points is

$$\delta_{\text{out}} = [R - \{\rho_j + \rho_r\}]. \tag{41}$$

In this expression, if $R < \{\rho_j + \rho_r\}$, compression takes place and restoring force act.

If $R > \{\rho_j + \rho_r\}$, no compression and restoring force is set equal to zero.

The radial internal clearance (γ_0) is the clearance between the imaginary circles, which circumscribe the rolling elements and the outer race. Hence, with the consideration of radial internal clearance (γ_0), the contact deformations at the inner and outer races are

$$\delta_{\text{in}} = [\{r + \rho_r + \gamma_0\} - \chi_j], \tag{42}$$

$$\delta_{\text{out}} = [R - \{\rho_j + \rho_r + \gamma_0\}]. \tag{43}$$

2.4. Equations of motion

The kinetic energy and potential energy contributed by the inner race, the outer race, rollers, rotor and springs, can be differentiated with respect to the generalized coordinates ρ_j $(j = 1, 2, \ldots, N_b)$, x_{in}, and y_{in} to obtain the equations of motion. For the generalized coordinates ρ_j, where $j = 1, 2, \ldots, N_b$, the equations are

$$m_j\ddot{\rho}_j + m_j g \sin\theta_j + m_j\rho_j\dot{\theta}^2 - (k_{\text{in}})[\delta_{\text{in}}]_+\frac{\partial\chi_j}{\partial\rho_j} + (k_{\text{out}})[\delta_{\text{out}}]_+ + \frac{1}{2}\frac{\partial k_{\text{in}}}{\partial\rho_j}[\delta_{\text{in}}]_+^2 + \frac{1}{2}\frac{\partial k_{\text{out}}}{\partial\rho_j}[\delta_{\text{out}}]_+^2 = 0, \quad j = 1, 2, \ldots, N_b. \tag{44}$$

For the generalized coordinate x_{in}, the equation is

$$(m_{\text{in}} + m_{\text{rotor}})\ddot{x}_{\text{in}} - \sum_{j=1}^{N_b} k_{\text{in}}[\delta_{\text{in}}]_+\frac{\partial\chi_j}{\partial x_{\text{in}}} = F_u \sin(\omega t). \tag{45}$$

For the generalized coordinate y_{in} the equation is

$$(m_{\text{in}} + m_{\text{rotor}})\ddot{y}_{\text{in}} + (m_{\text{in}} + m_{\text{rotor}})g - \sum_{j=1}^{N_b} k_{\text{in}}[\delta_{\text{out}}]_+\frac{\partial\chi_j}{\partial y_{\text{in}}} = W + F_u \cos(\omega t). \tag{46}$$

This is a system of $(N_b + 2)$ second-order, nonlinear differential equations. No external radial force is allowed to act on the bearing system and no external mass is attached to the outer race. The "+" sign as subscript in these equations signifies that if the expression inside the bracket is greater than zero, then the rolling element at angular location θ_j is loaded giving rise to restoring force, and if the expression inside the bracket is negative or zero, then the rolling element is not in the load zone, and restoring force is set to zero. For the balanced rotor condition, the unbalance rotor force (F_u) is set to be zero.

The deformation of spring at inner race χ_j (Fig. 2) can be obtained as

$$x_{\text{in}} + \chi_j \cos\theta_x = x_{\text{out}} + \rho_j \cos\theta_j, \tag{47}$$

$$y_{\text{in}} + \chi_j \sin\theta_x = y_{\text{out}} + \rho_j \sin\theta_j. \tag{48}$$

From these two equations, the expression for χ_j is obtained as

$$\chi_j = [(x_{\text{out}} - x_{\text{in}})^2 + \rho_j^2 + 2\rho_j(x_{\text{out}} - x_{\text{in}})\cos\theta_j + 2\rho_j(y_{\text{out}} - y_{\text{in}})\sin\theta_j + (y_{\text{out}} - y_{\text{in}})^2]^{1/2}. \tag{49}$$

Now the partial derivatives of χ_j with respect to ρ_j, x_{in} and y_{in} are

$$\frac{\partial\chi_j}{\partial\rho_j} = \frac{\rho_j + (x_{\text{out}} - x_{\text{in}})\cos\theta_j + (y_{\text{out}} - y_{\text{in}})\sin\theta_j}{\chi_j}, \tag{50}$$

$$\frac{\partial\chi_j}{\partial x_{\text{in}}} = \frac{(x_{\text{out}} - x_{\text{in}}) - \rho_j\cos\theta_j}{\chi_j}, \tag{51}$$

$$\frac{\partial \chi_j}{\partial y_{\text{in}}} = \frac{(y_{\text{out}} - y_{\text{in}}) - \rho_j \sin \theta_j}{\chi_j}. \tag{52}$$

The nonlinear stiffness of spring for the inner and the outer race obtained by Eq. (13) is

$$(k_{\text{in}}) = 56065.703 \times l_{\text{eff}}^{0.92} \delta_{\text{in}}^{0.08} \quad (\text{N/mm}), \tag{53}$$

$$(k_{\text{out}}) = 56065.703 \times l_{\text{eff}}^{0.92} \delta_{\text{out}}^{0.08} \quad (\text{N/mm}), \tag{54}$$

$$\frac{(\partial k_{\text{in}})}{\partial \rho_j} = -4485.256 \times [\delta]_{\text{in}}^{-0.92} (l_{\text{eff}}^{0.92}) \frac{\partial \chi_j}{\partial \rho_j}, \tag{55}$$

$$\frac{(\partial k_{\text{out}})}{\partial \rho_j} = -4485.256 \times [\delta]_{\text{out}}^{-0.92} (l_{\text{eff}}^{0.92}). \tag{56}$$

3. Computational solution of the equations

The equations of motion (44–46) are solved by the modified Newmark-β method to obtain the radial displacement and velocity of the rolling elements. In order to eliminate the effect of the natural frequency an artificial damping was introduced into the system. With this damping, transient vibrations are eliminated. Thus, peak steady-state amplitude of vibration can be measured. The longer the time to reach steady-state vibrations, the longer the CPU time needed, and hence the more expensive the computation. A value of $c = 320\,\text{Ns/m}$ is chosen. To study the stability of the system, parameters of rolling bearing are selected as shown in Table 1.

3.1. Initial conditions

For the numerical technique used, the initial conditions and step size are very important for a good and computationally inexpensive solution. Particularly for nonlinear systems,

Table 1
Geometric and physical properties used for the rolling bearings

Mass of rolling element (m_j)	0.06 kg
Mass of the inner race (m_{in})	0.09 kg
Mass of the outer race (m_{out})	0.09 kg
Mass of rotor (m_{rotor})	0.6 kg
Length over which the rollers are actually in contact—rolling rearing only (l_{eff})	8 mm
Internal radial clearance (γ)	20 μm
Maximum amplitude of waviness (Π_p)	2 μm
Initial amplitude of waviness (Π_0)	1 μm
No. of rolling elements (N_r)	8
No. of wave lobes (N_w)	8
Initial radial position of jth rolling element (ρ_j)	27 mm
Radial load (W)	6 N

different initial conditions mean a totally different system and hence different solutions. The larger the time step, Δt, the faster is the computation. On the other hand, the time step should be small enough to achieve accuracy. However, very small time steps can increase the truncation errors. The Newmark-β method has a provision for estimating local truncation error. For various speeds and $W = 6\,\mathrm{N}$, the system is numerically integrated on a Silicon Graphics workstation for a number of time step sizes. The local truncation error and CPU time are plotted against the time step as shown in Fig. 4. One can see that region A–A′ gives the best results. Therefore an optimization should be made between them. The time step for the investigation is taken to be $\Delta t = 10^{-5}\,\mathrm{s}$. The non-autonomous shooting method is used for finding out the fixed point of the steady-state solution. The fixed point is used as the initial condition for numerical integration results in a steady-state solution with no transient. When some arbitrary initial conditions are taken, transients are formed, which take some time to die down. For the nonlinear system the transients may lead to instability. On taking fixed point as initial conditions, the transients are not formed resulting in the saving of a considerable computational time. At time $t = 0$ the following assumptions are made:

(i) The shaft is held at the center of the bearing and all rollers are assumed to have equal radial preload.
(ii) The shaft is then given initial displacements and velocities. For fast convergence the initial displacements are set to the following values: $x_0 = 10^{-6}\,\mathrm{m}$ and $y_0 = 10^{-6}\,\mathrm{m}$. The initial velocities are assumed to be zero: $\dot{x}_0 = 0$ and $\dot{y}_0 = 0$.
(iii) When $t > \Delta t$ the initial conditions have already passed and the normal procedure commences.

Rolling elements are radially preloaded in order to ensure the continuous contact of all rolling elements and the raceways, otherwise a chaotic behavior might be observed.

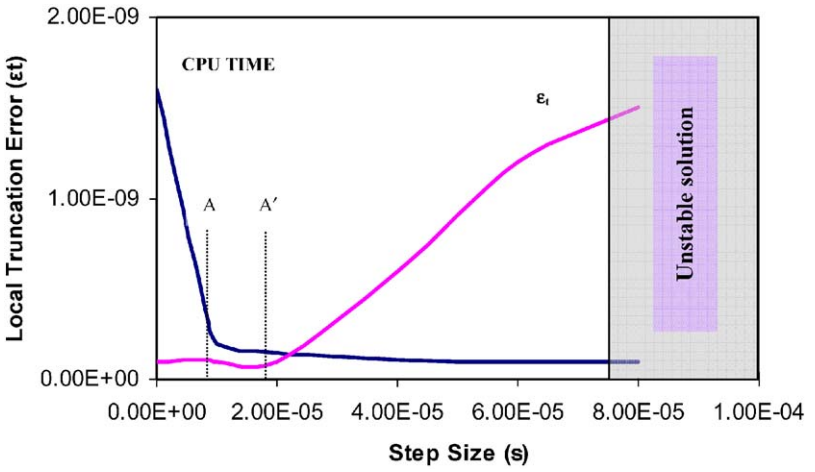

Fig. 4. Effect of step size on stability of system.

3.2. Power spectra and Poincarè maps

The time history of the unbalance responses has been examined for periodic behavior. This is done by examining the time series output, once per cycle, for sufficiently long segments so that multiple periodic and aperiodic behaviors can be discerned from the post-transient solutions. Frequency spectra and Poincarè maps are generated for studying the stability and nature of the solution. Aperiodic behavior in a deterministic dynamical system is characterized by broadband frequency spectra. In sub-synchronous frequencies, the significant energy shows the aperiodic nature of the response. Poincarè maps are produced by plotting one of the variables of the system, e.g. the vertical or horizontal displacement, against its derivative, once per rotational periodic of the system. For synchronous limit cycle a single point in the plane is repeated every cycle, while nth sub-harmonic is revealed by n and only n repeated points. However, Poincarè maps of the chaotic system have a fractal structure, which can be used to identify chaotic states.

4. Results and discussion

In this work, besides speed as a parameter of study, the effect of radial internal clearance and surface waviness is also studied. Both are important parameters of study because even if these are inevitable, these can be controlled to a good extent. Speed response plots are obtained for the combination of the above parameters under study. These plots are generated by numerical integration to reach steady state when peak-to-peak (pp) values of x and y displacements are obtained. The overall response plot of rolling element bearing for *line* contact with radial clearance 1 μm and radial load of 6N is shown in Fig. 5. The peak-to-peak vertical response is less than the peak-to-peak horizontal response in the region of high amplitude. The overall response plot has a very rough appearance. Two regions can be identified, which have high pp response.

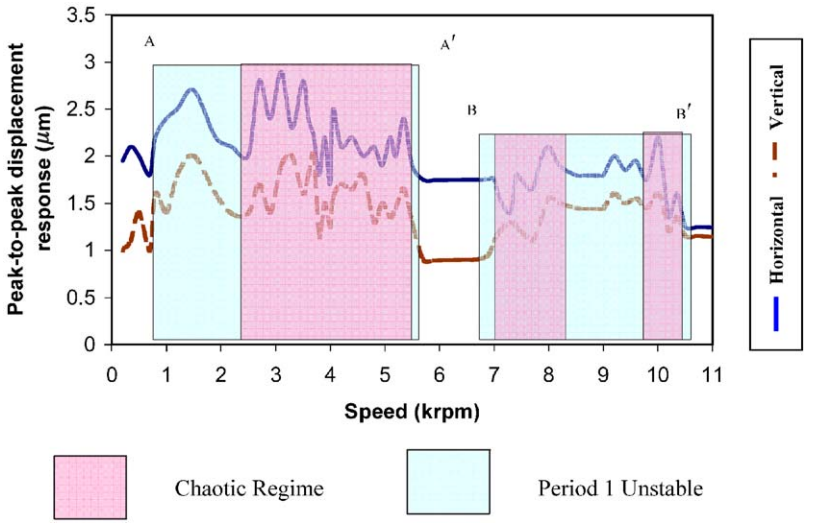

Fig. 5. Response plot for $\gamma_0 = 1\,\mu\text{m}$ and $W = 6\,\text{N}$.

Table 2
Nature of solutions for $\gamma_0 = 1\,\mu m$, $W = 6\,N$

Speed (rev/min)	Nature of solution
Upto 775	1T stable low amplitude
780–1900	Period 1 unstable (at VC and harmonics)
1950–2200	Chaos developing
2350–5640	Chaotic
5700–6885	Periodic
6990–8170	Chaotic
8200	Chaotic natures decreasing
8500–9700	Period 1 unstable (mixed nature)
9750–10020	Intermittent Chaotic
10030–10300	Chaotic
10350	Periodic

These regions are shown in Fig. 5 bounded by lines A–A′ and B–B′. The nature of solutions for various speeds is given in Table 2.

Two regions of period 1 unstable response are shown in Fig. 5. The first region from 780 to 5615 rev/min has period doubling bifurcations. This is also a multi-valued region. The eigenvalues of the monodromy matrix go out through −1. Fig. 6 shows the nature of the solution at 1500 rev/min. The VC and its harmonics (super-harmonic) character of the frequency spectra is also brought out by the Poincarè map. The chaos is at the developing stage from 1950 rev/min. The phase plot also shows that more dense orbits points are surrounded by less dense points. Fig. 7 shows the nature of solution at 2200 rev/min. In the frequency spectrum a band structure is seen in between spikes of VC and its multiples. The fine-layered structure of the strange attractor is also clear from the Poincarè map. As speed increases, the chaotic region appears at 2350–5640 rev/min; the loss of stability is seen to be caused by the eigenvector crossing from +1. In this region, the periodic doubling bifurcations give way to chaos at about 2400 rev/min and this chaotic region extends upto 5640 rev/min. The chaotic solutions at 2500, 3800, 4000, 4050, 5100 and 5200 rev/min are shown in Figs. 8–13. The frequency spectrum has a dense band structure as shown in between spikes of VC and its multiples. The fine-layered structure of the strange attractor is also clear from Poincarè maps. The orbit at this speed does not repeat itself. The Poincarè maps of chaotic solutions have fractal structures that repeat as the maps are magnified. The route to chaos by sudden loss of stability through a limit point has been shown by Sankarvelu et al. [7]. The chaotic region seems to be at end stage from 5400 rev/min as shown in Fig. 14. Further increase in speed returns stability in the speed range from 5500 to 6885 rev/min.

The second region from 6915 to 10 350 rev/min has period doubling bifurcations as shown in Fig. 5. This is also a region of multi-valued region. Period one solution becomes unstable from 6915 to 10 350 rev/min, because of periodic doubling bifurcations. The solution undergoes pitchfork bifurcations till 6950 rev/min after which at 6990 rev/min the chaotic solution is obtained. Fig. 15 shows the nature of solution at 7000 rev/min. In the frequency spectrum a band structure is seen in between spikes of VC and its multiples. The fine-layered structure of the strange attractor is also clear from Poincarè maps.

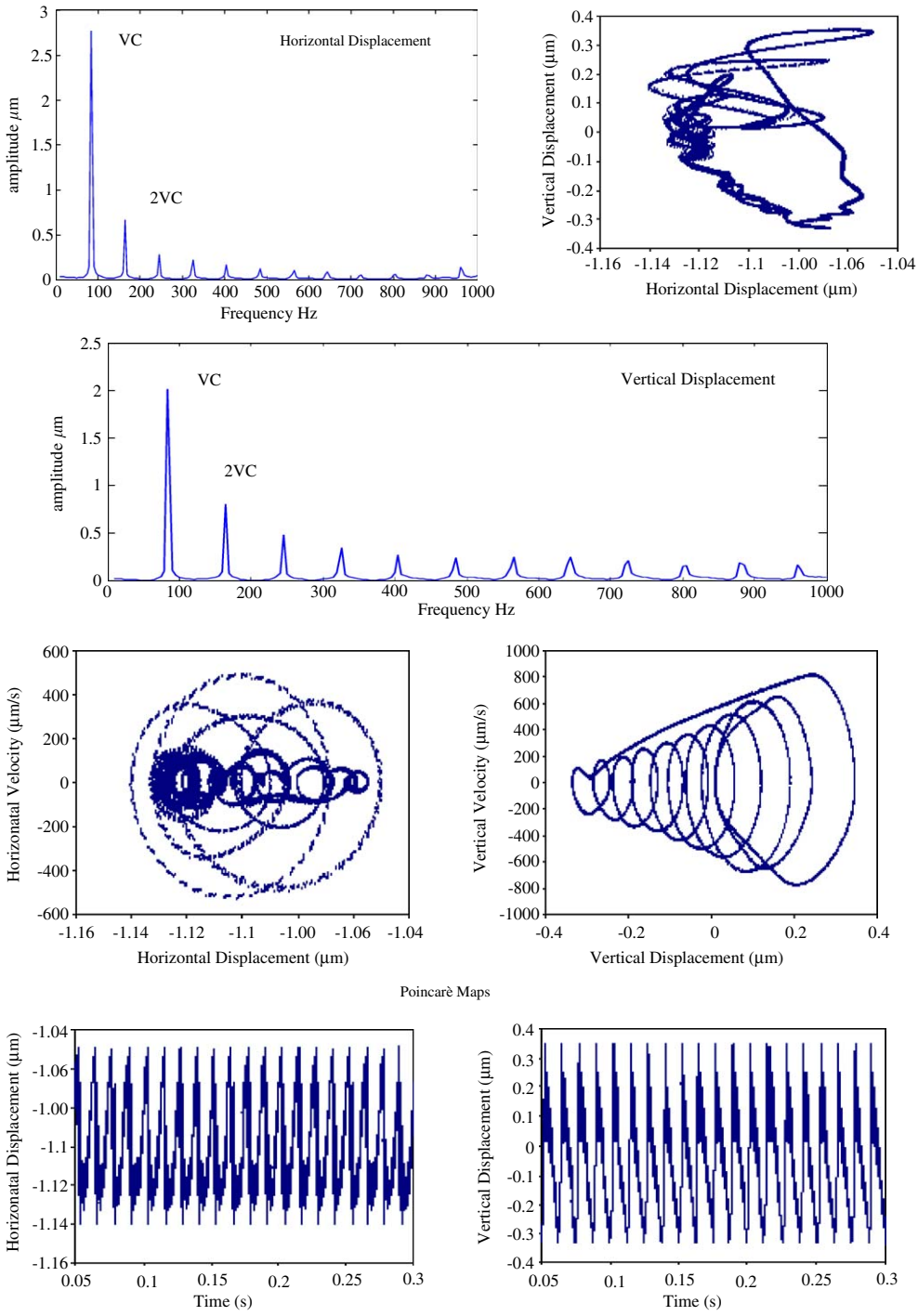

Fig. 6. Response at 1500 rev/min for $\gamma_0 = 1\,\mu\text{m}$, $W = 6\,\text{N}$.

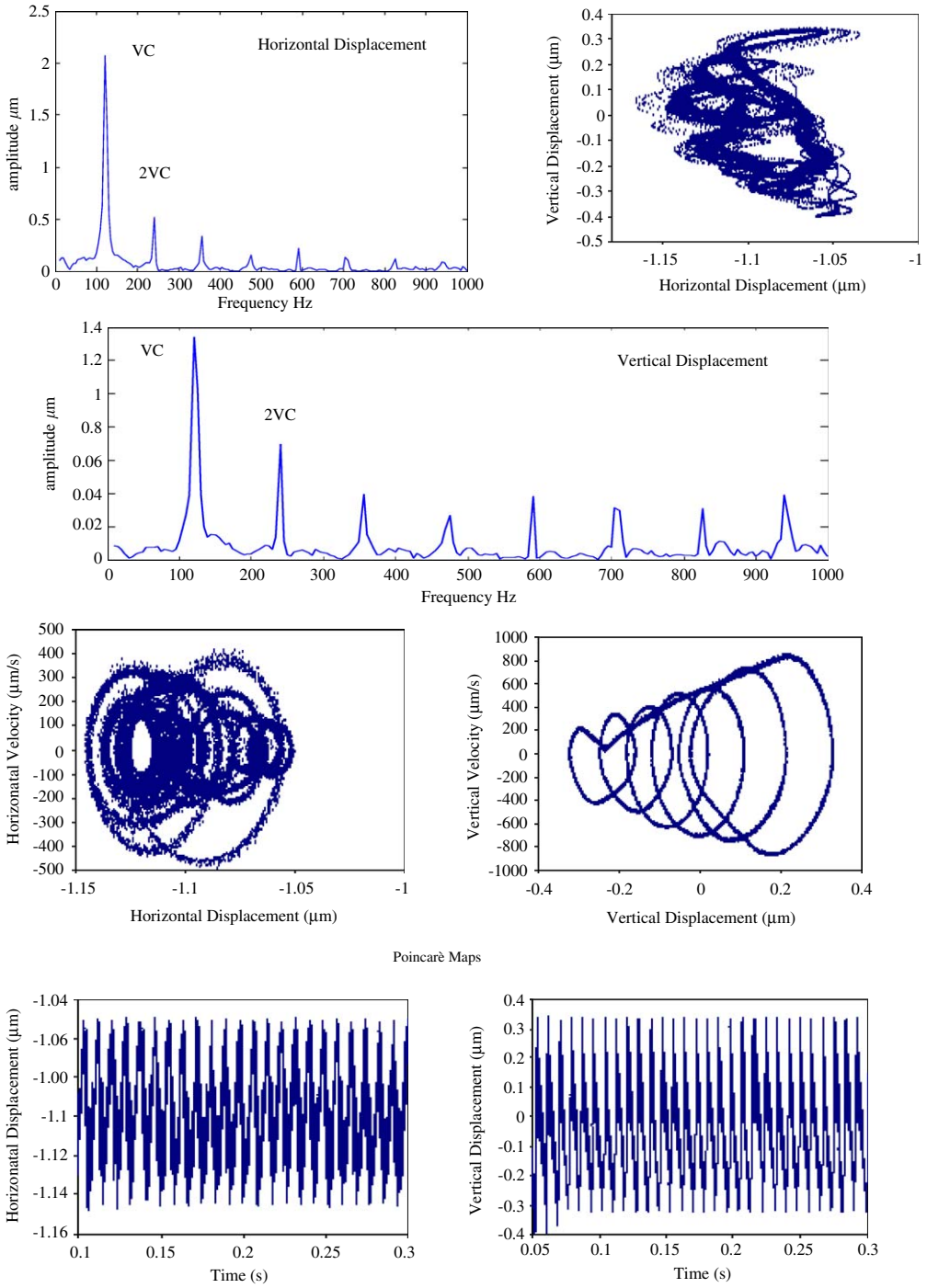

Fig. 7. Response at 2200 rev/min for $\gamma_0 = 1\,\mu\text{m}$, $W = 6\,\text{N}$.

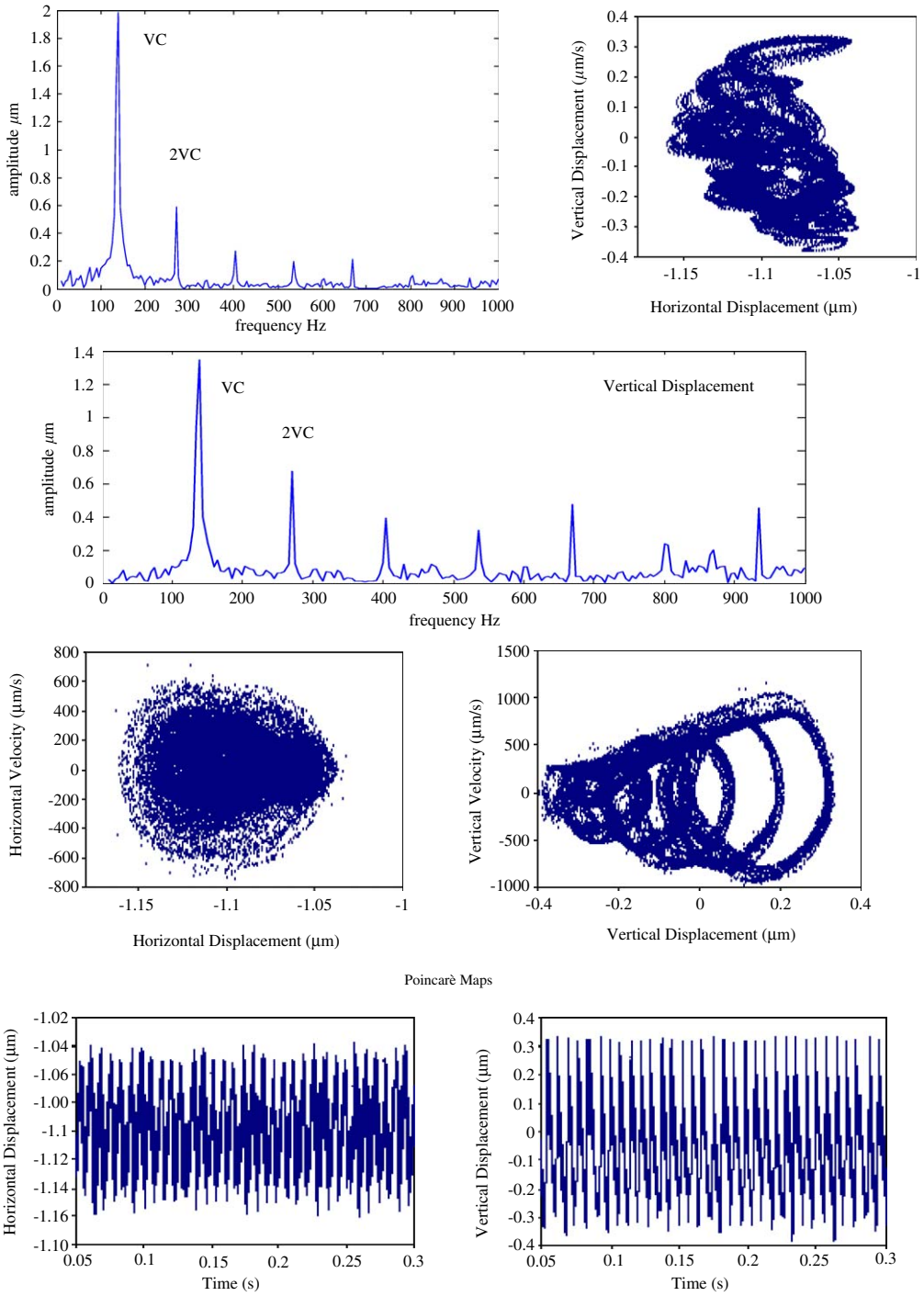

Fig. 8. Response at 2500 rev/min for $\gamma_0 = 1\,\mu\text{m}$, $W = 6\,\text{N}$.

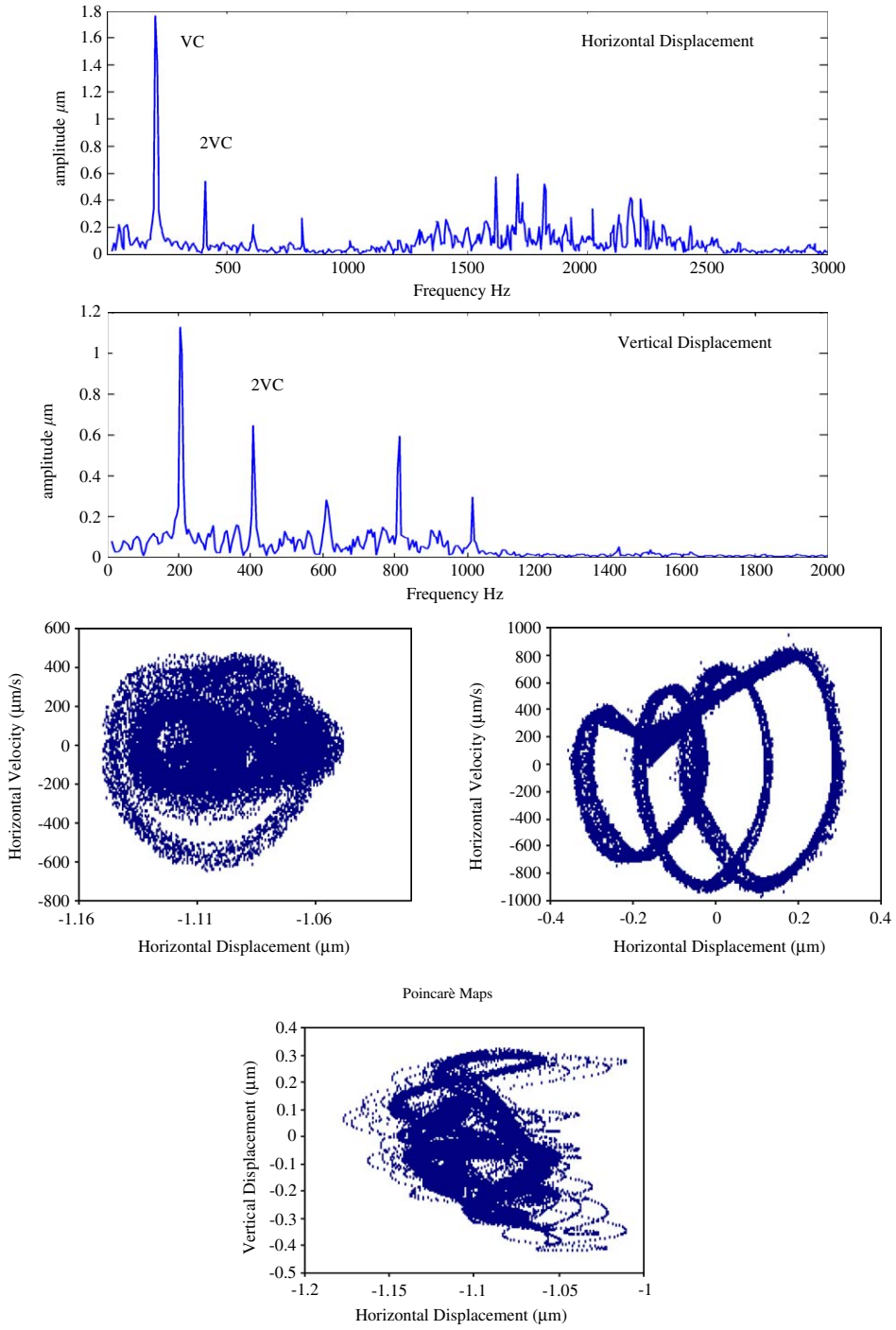

Fig. 9. Response at 3800 rev/min for $\gamma_0 = 1\,\mu\text{m}$, $W = 6\,\text{N}$.

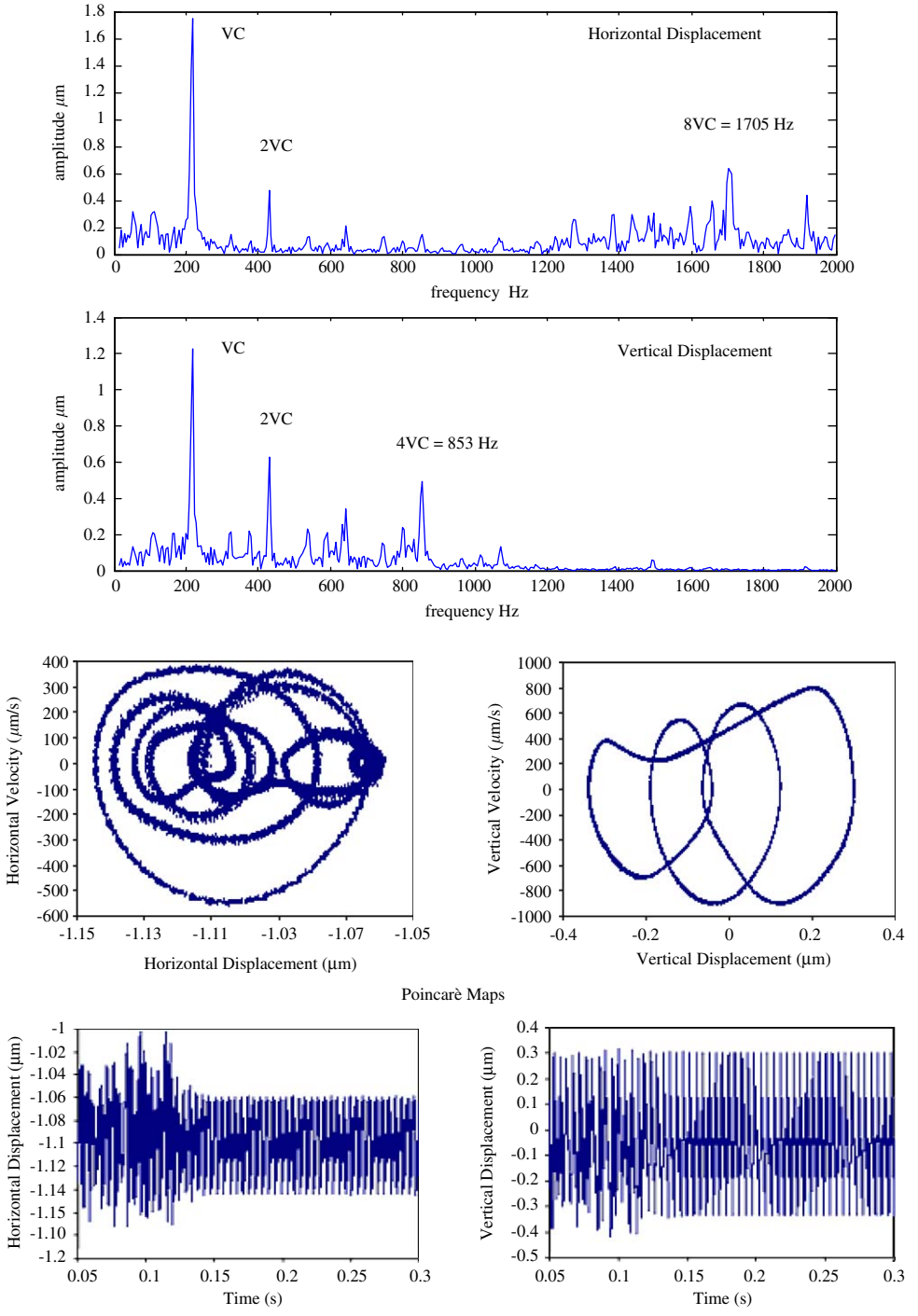

Fig. 10. Response at 4000 rev/min for $\gamma_0 = 1\,\mu\text{m}$, $W = 6\,\text{N}$.

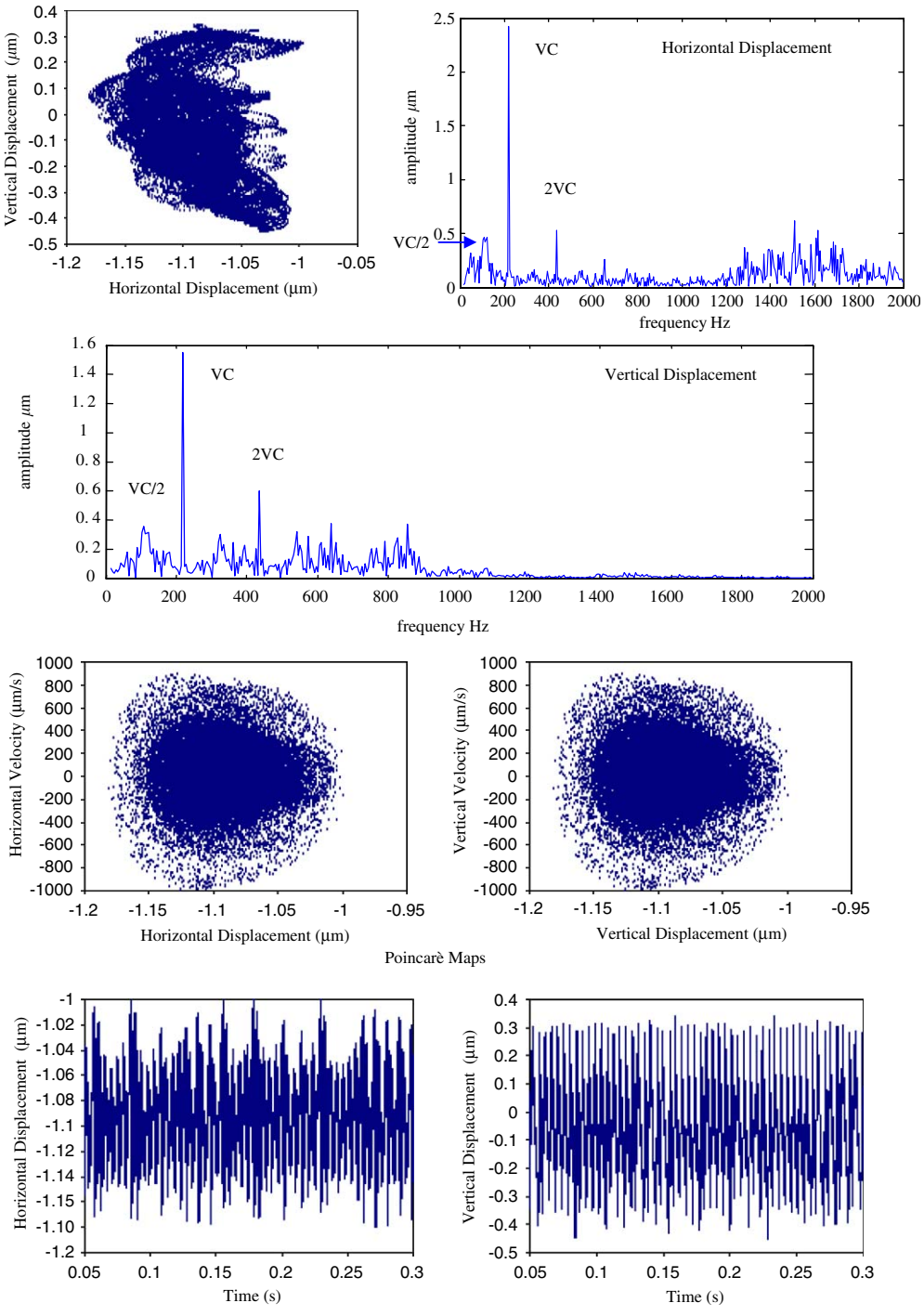

Fig. 11. Response at 4050 rev/min for $\gamma_0 = 1\,\mu m$, $W = 6\,N$.

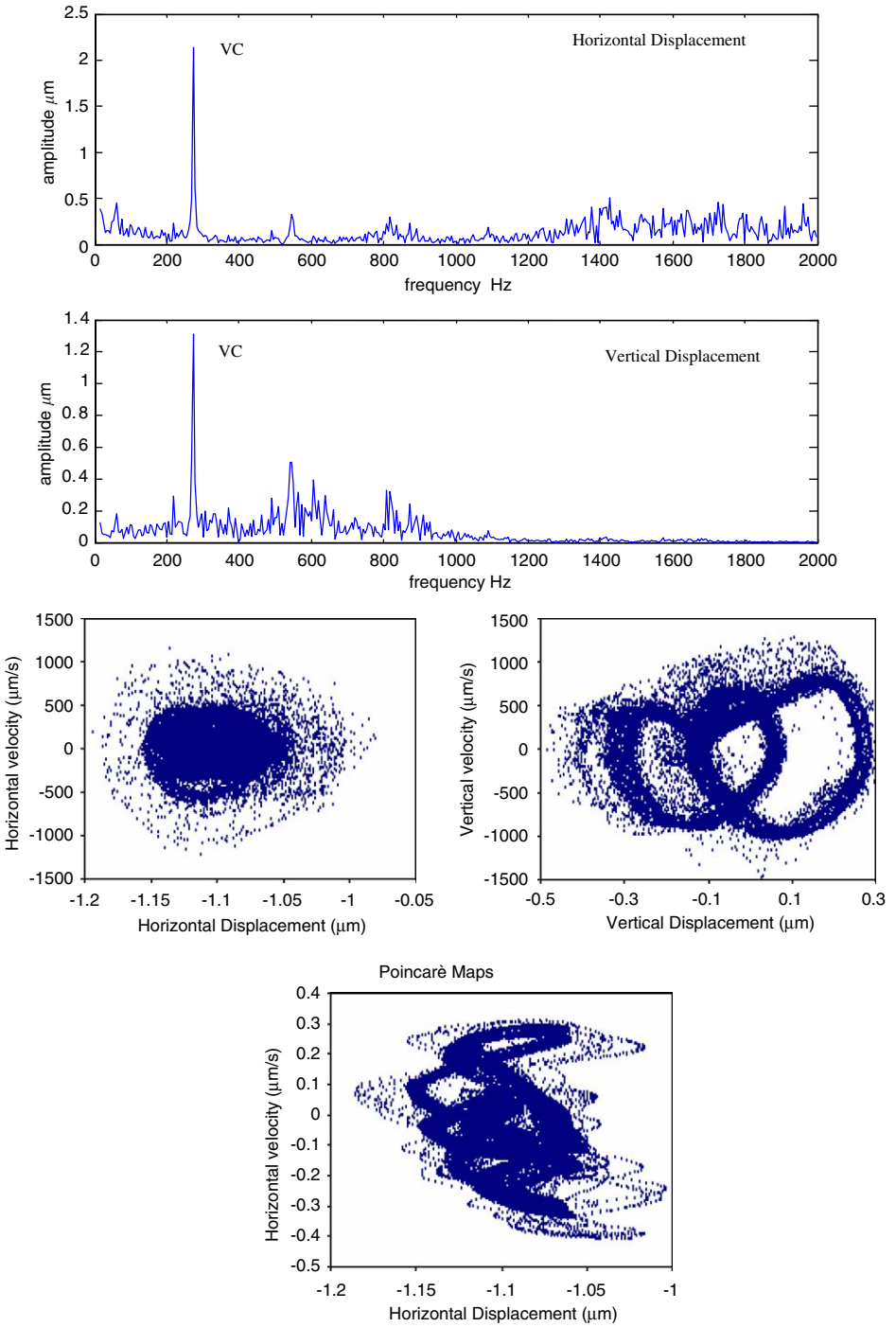

Fig. 12. Response at 5100 rev/min for $\gamma_0 = 1\,\mu\text{m}$, $W = 6\,\text{N}$.

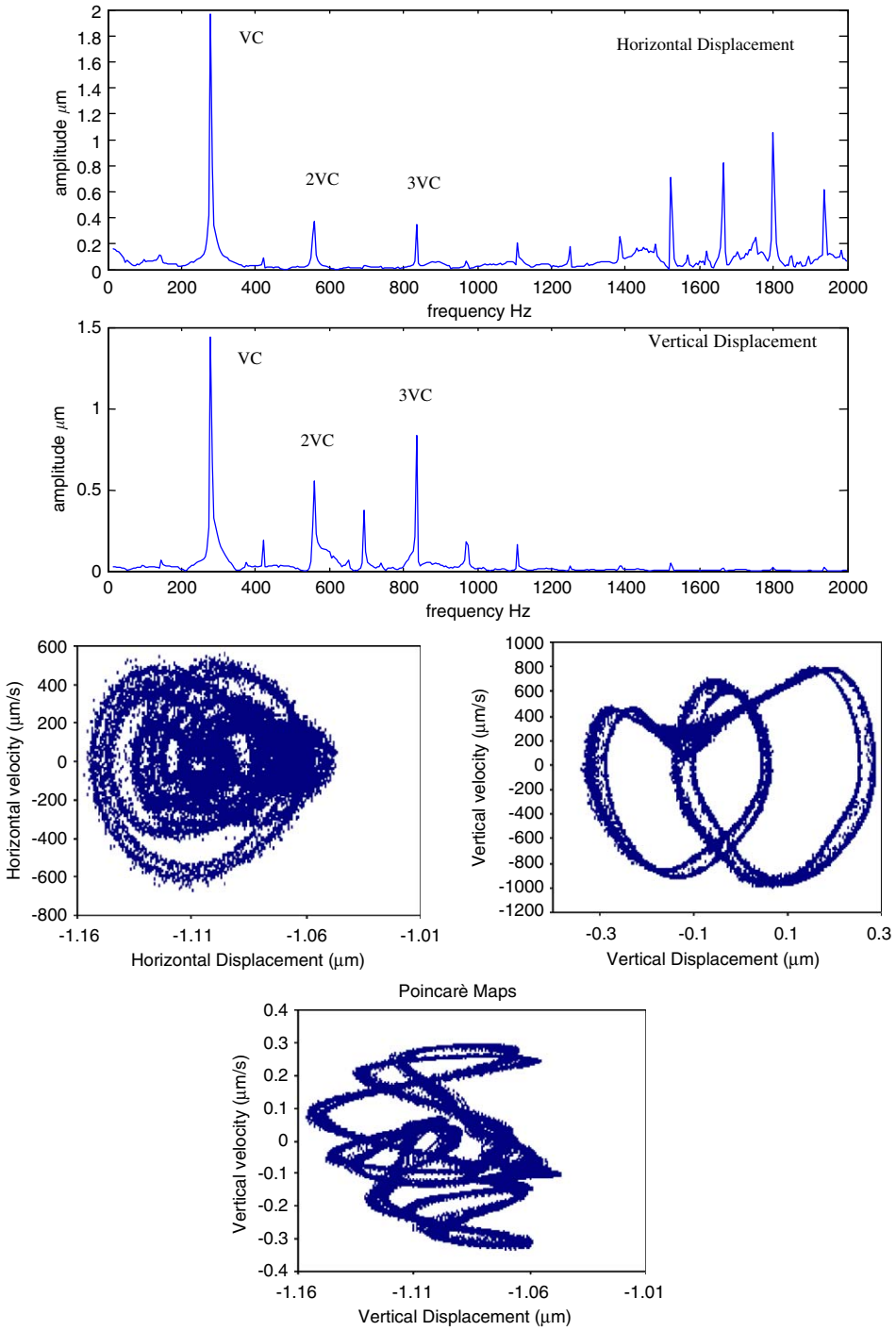

Fig. 13. Response at 5200 rev/min for $\gamma_0 = 1\,\mu\text{m}$, $W = 6\,\text{N}$.

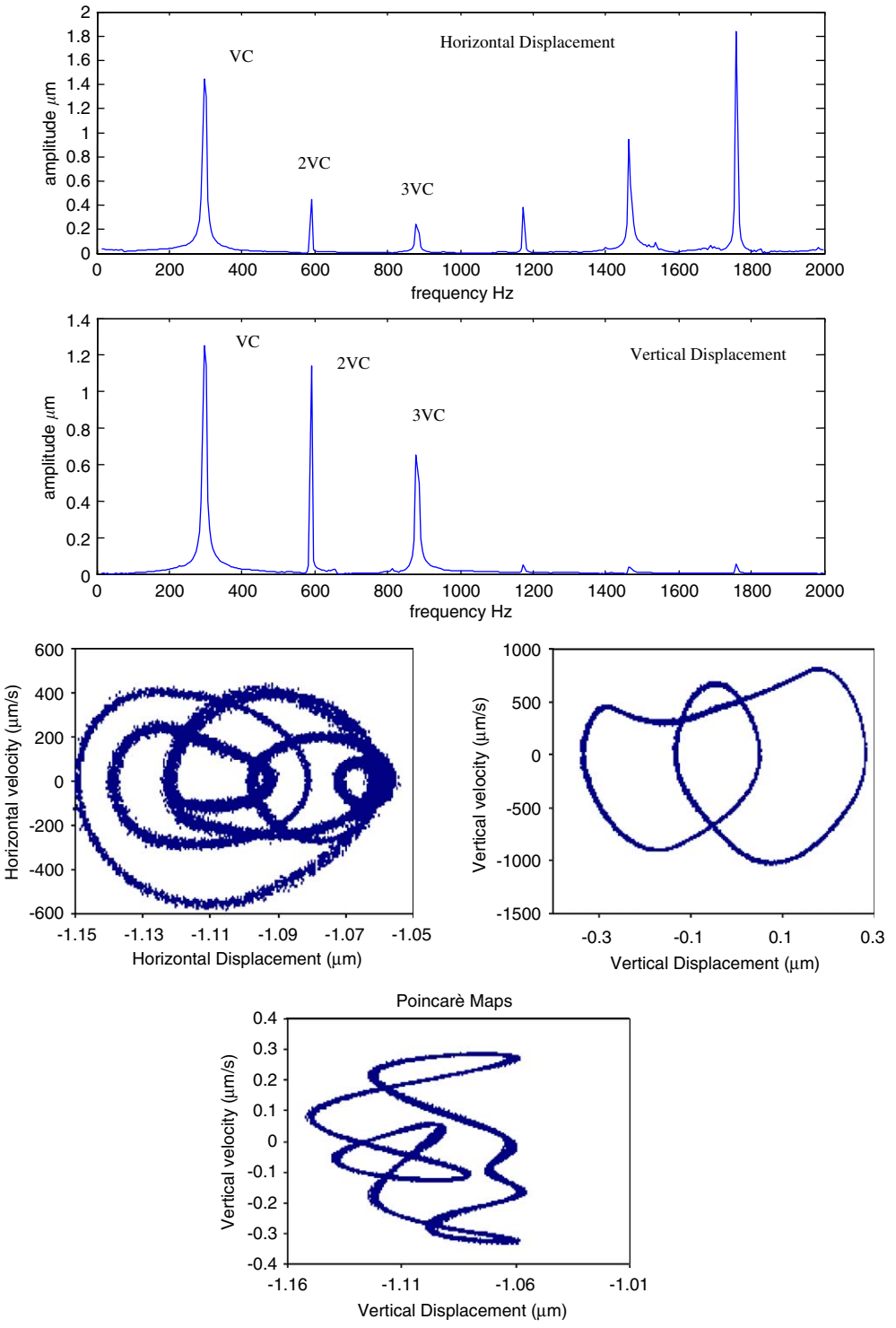

Fig. 14. Response at 5400 rev/min for $\gamma_0 = 1\,\mu\text{m}$, $W = 6\,\text{N}$.

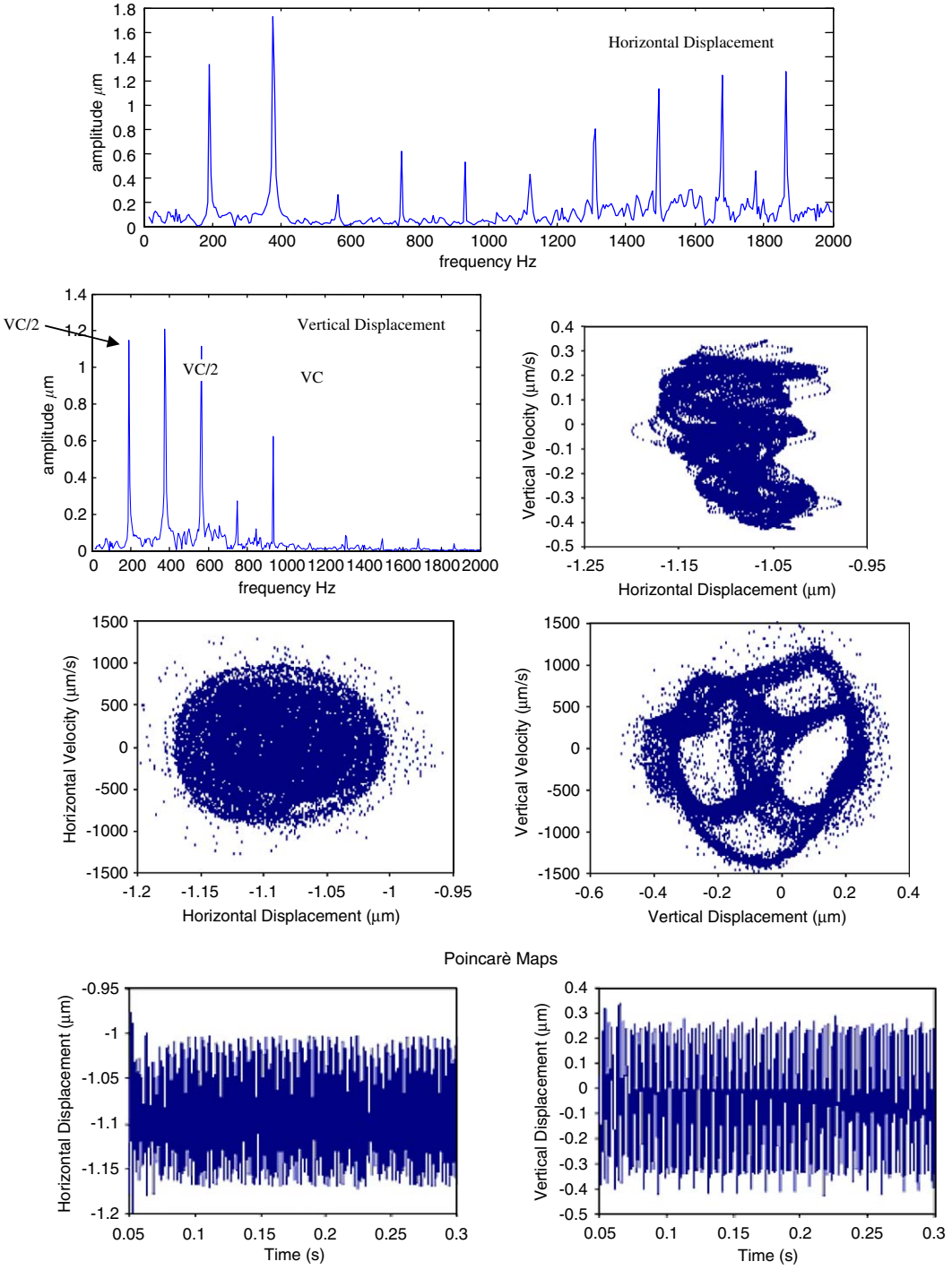

Fig. 15. Response at 7000 rev/min for $\gamma_0 = 1\,\mu\text{m}$, $W = 6\,\text{N}$.

For the first chaotic region 6990–8270 rev/min, the loss of stability is seen to be caused by the eigenvector crossing from +1. In this region, the periodic doubling bifurcations give way to chaos at about 6990 rev/min and this chaotic region extends upto 8270 rev/min. The chaotic solutions at 7100, 7500 and 8000 rev/min are shown in Figs. 16–18, respectively. The frequency spectrum has a dense band structure as shown in between spikes of VC and its multiples. The fine-layered structure of the strange attractor is also clear from Poincarè maps. The orbit at this speed does not repeat itself. The Poincarè maps of chaotic solutions have fractal structures that repeat as the map is magnified. The time responses also show beat- and chaos-like behavior. It is clear that loss of periodicity is one characteristic of chaotic solution. The response characteristic at 8200 rev/min is shown in Fig. 19. The horizontal and vertical displacement spectra (Fig. 19) have banded structure and orbit with dense and less dense regions. Analysis has shown that the chaotic character becomes weaker from 8270 rev/min onwards. At 8500 rev/min, the response shown in Fig. 20 can be considered neither perfectly chaotic nor perfectly periodic. It is not perfectly or predominantly chaotic because the two spectra for horizontal and vertical displacements have only a slightly banded structure. The orbits in Poincarè maps are complicated because of this mixed nature of the response.

At 10 000 rev/min, the response explodes into intermittent behavior. The eigenvalues of monodromy matrix cross from +1, so this becomes an intermittent behavior of type I. In Fig. 21, the frequency spectra show the band structure and the orbit shows a small dense region surrounded by a less dense structure. As speed increases, the second chaotic region appears between 10 030 and 10 300 rev/min, the loss of stability is seen to be caused by the eigenvector crossing from +1. In this region, the periodic doubling bifurcations give way to chaos at about 10 030 rev/min and this region extends upto 10 300 rev/min. Further increase in speed returns perfect stability in the speed range from 10 350 rev/min onwards. Also the peak-to-peak (pp) response goes down (Fig. 5), which is an indication of the end of the multi-valued region of response.

5. Conclusions

The nonlinear response of a balanced rotor with internal radial clearance and surface waviness has been demonstrated to be chaotic for some specific combination of unbalance and rotational speed combined with a misalignment of races to provide sufficient nonlinearity. For cases, which are stable to free motion and not close to the neutral stability line, a limited range of chaos can be detected. From the study of the response, the following conclusions can be drawn.

(1) The rotor-bearing system has three high amplitude regions. The first region is one of periodic doubling response where the period one response is unstable. This region also has bifurcations leading to 1T and 2T solutions. Chaotic responses appear in this region, which has a strong attractor as compared to chaotic behavior in other regions. As Fukata et al. [5] have shown, this region forms around horizontal critical speeds.
(2) The effect of the high-speed rotor results in a larger unstable region in roller bearing. Both regions of unstable response also show the occurrence of chaos for high-speed rotor. Invariably, the route to chaos is seen to be intermittency mechanism by period doubling behavior.

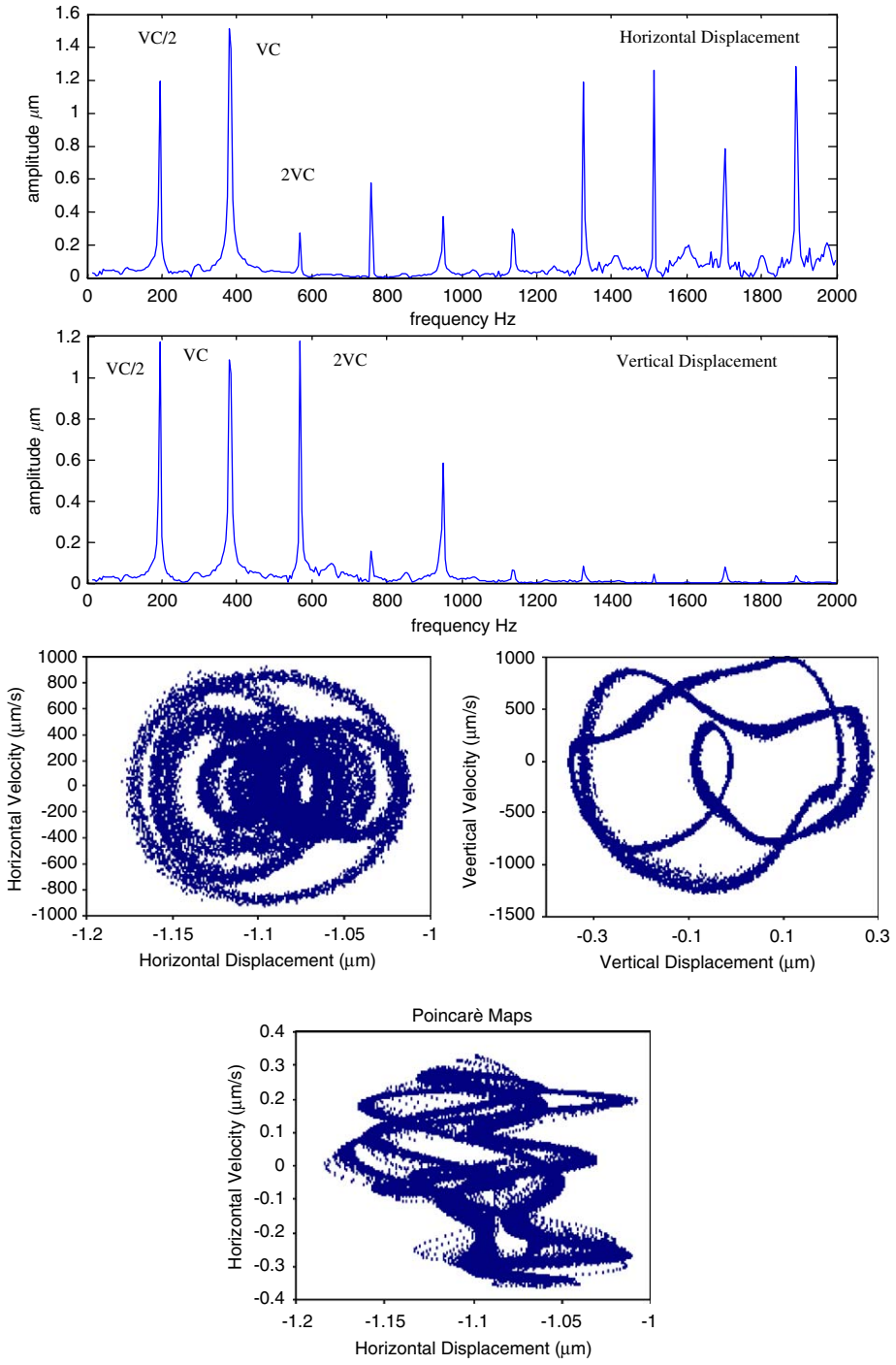

Fig. 16. Response at 7100 rev/min for $\gamma_0 = 1\,\mu\text{m}$, $W = 6\,\text{N}$.

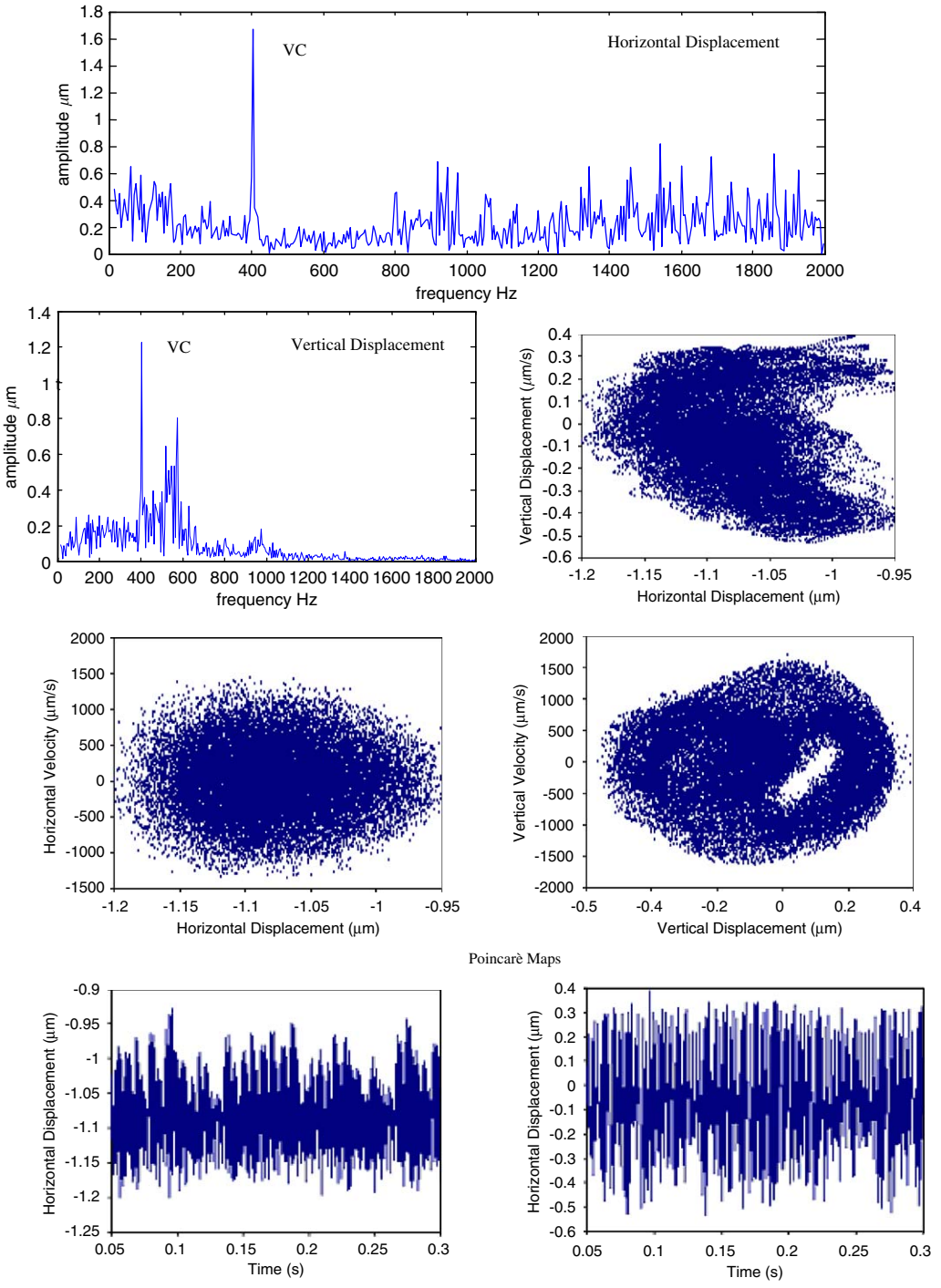

Fig. 17. Response at 7500 rev/min for $\gamma_0 = 1\,\mu\text{m}$, $W = 6\,\text{N}$.

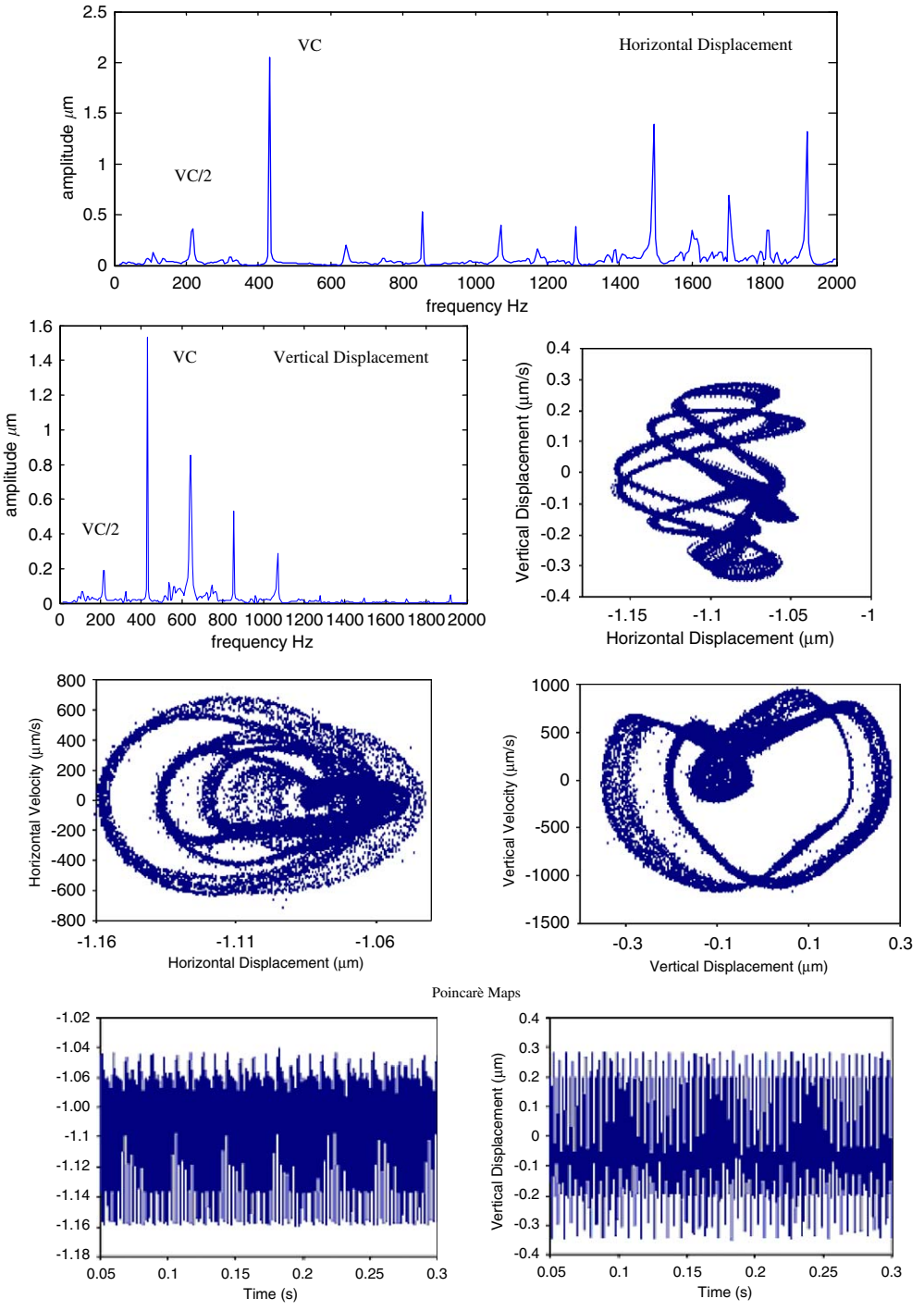

Fig. 18. Response at 8000 rev/min for $\gamma_0 = 1\,\mu\text{m}$, $W = 6\,\text{N}$.

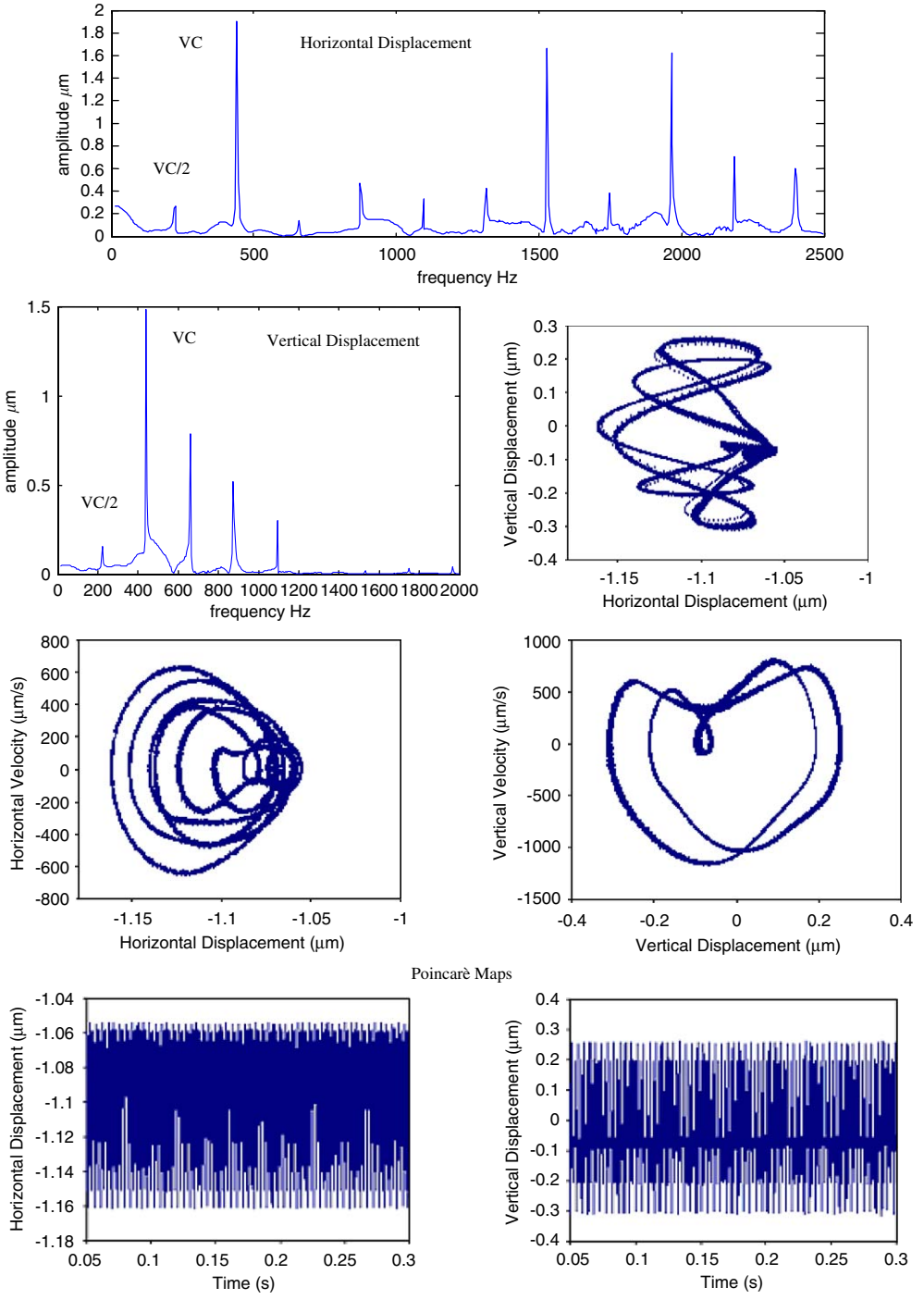

Fig. 19. Response at 8200 rev/min for $\gamma_0 = 1\,\mu\text{m}$, $W = 6\,\text{N}$.

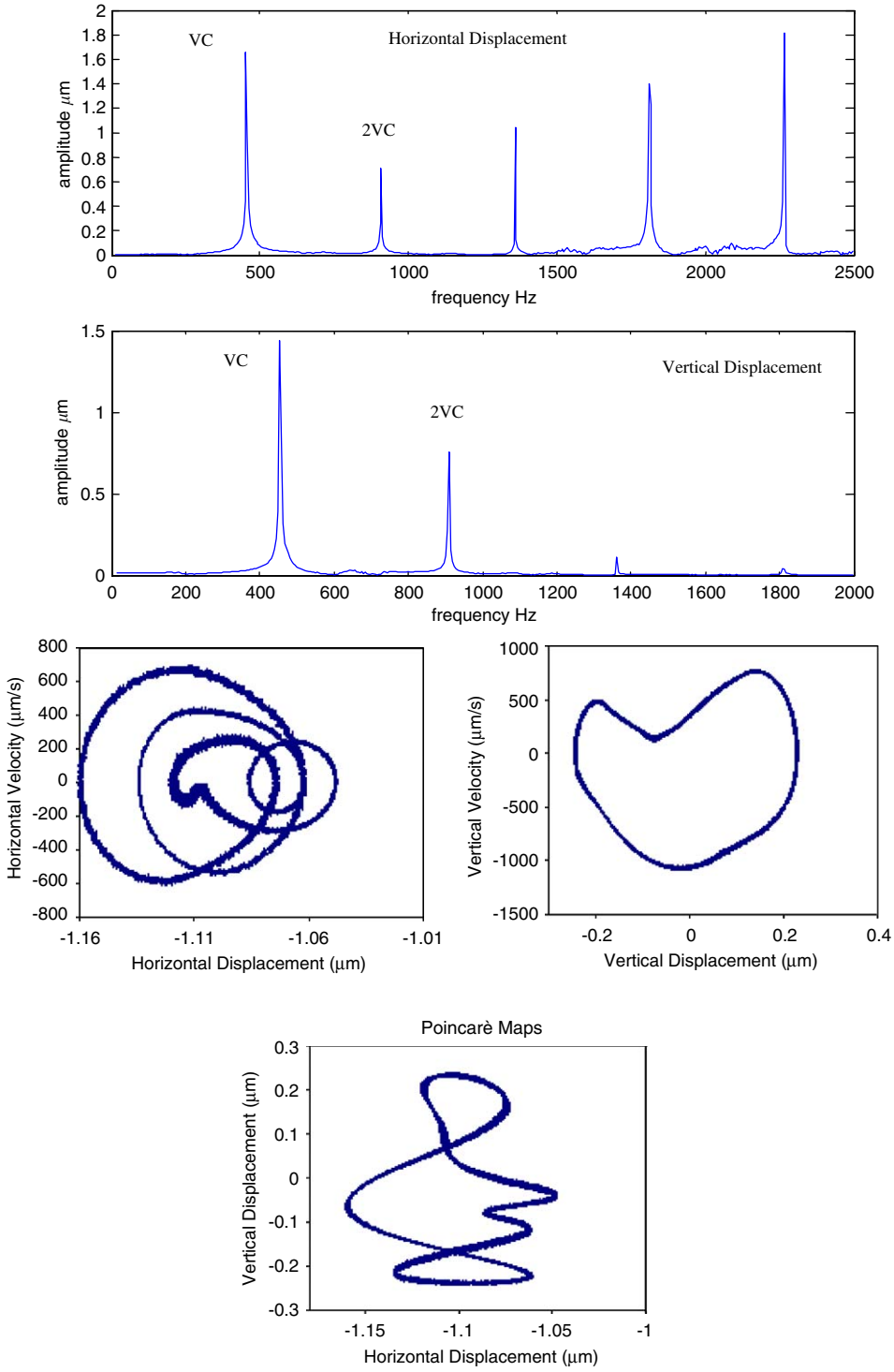

Fig. 20. Response at 8500 rev/min for $\gamma_0 = 1\,\mu\text{m}$, $W = 6\,\text{N}$.

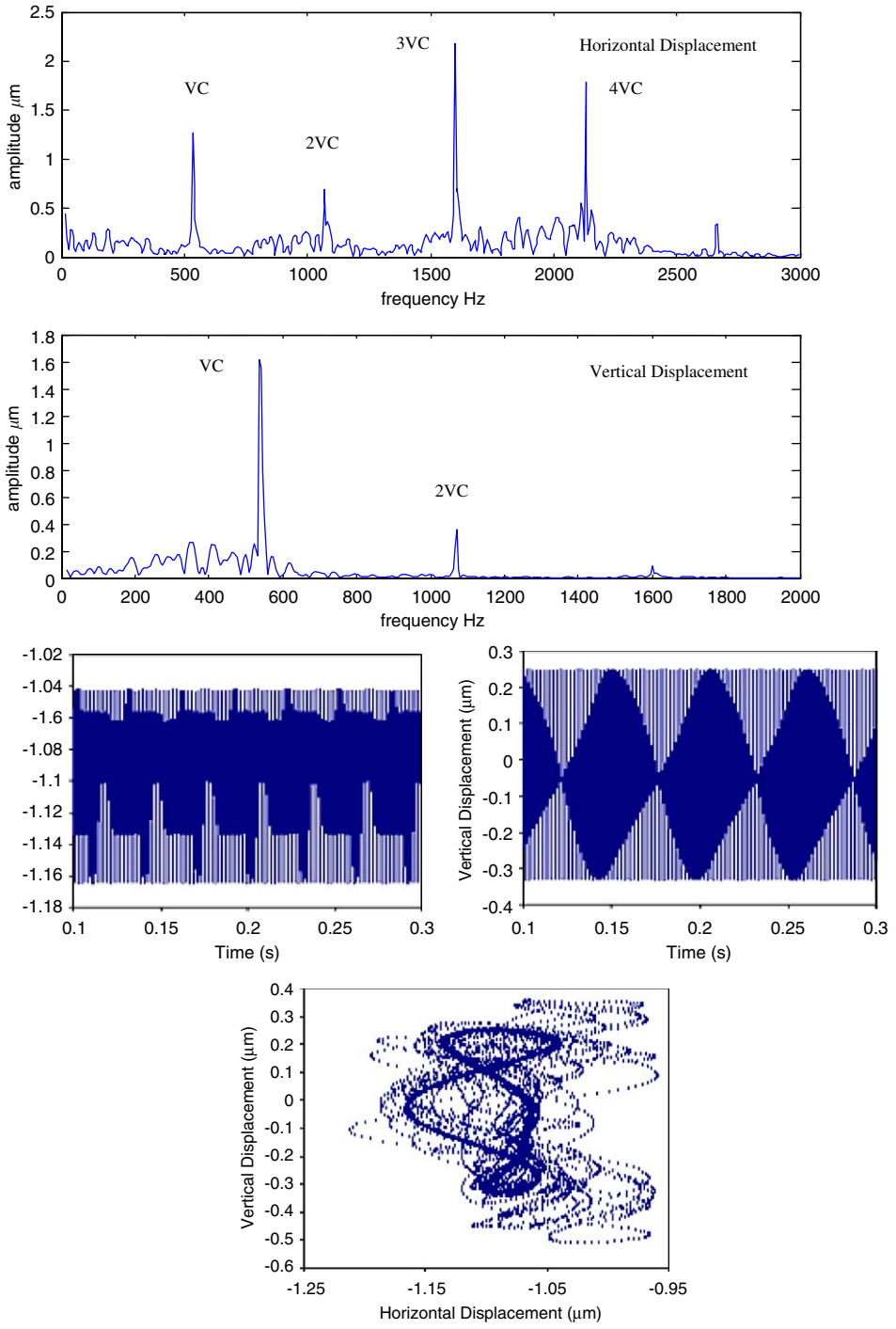

Fig. 21. Response at 10 000 rev/min for $\gamma_0 = 1\,\mu\text{m}$, $W = 6\,\text{N}$.

(3) Based on the characteristics of the dynamic behavior of the system, the responses may be put into three categories. (i) The system responses are periodic. This is a well-behaved region, which helps the designer to predict the trends accurately and without ambiguity. (ii) The system responses are of mixed nature. The horizontal and vertical displacement spectra show a banded structure and there are closed orbits with dense and not so dense regions. The response can be considered neither perfectly chaotic nor perfectly periodic. It is not perfectly or predominantly chaotic because the two spectra for horizontal and vertical displacements have only a slightly banded structure. The orbits in Poincarè maps are complicated because of this mixed nature of the response. For these responses, the hidden danger is the periodicity. The periodic response may lead designers to overlook its large sensitivity to small variations of system parameters or operating conditions. (iii) The responses are chaotic. The Poincarè maps of chaotic response have a fractal structure that repeats as the map is magnified. The time responses also show beat- and chaos-like behavior. It is clear that loss of periodicity is one characteristic feature of the chaotic solution.

References

[1] T. Yamamoto, On the vibration of a shaft supported by bearing having radial clearances, *Transactions of JSME* 21 (1955) 182–192.

[2] H. Perret, Elastic Spielschwingungen Konstant Walzlger, *Werkstalt und Betrieb* 3 (1950) 354–358.

[3] E. Meldau, Die Bewegung der Achse von Wälzlagern bei geringen Drehzahlen, *Werkstalt und Betrieb* 7 (1951) 308–313.

[4] C.S. Sunnersjo, Varying compliance vibrations of rolling bearings, *Journal of Sound and Vibration* 58 (1978) 363–373.

[5] S. Fukata, E.H. Gad, T. Kondou, T. Ayabe, H. Tamura, On the radial vibrations of ball bearings (computer simulation), *Bulletin of the JSME* 28 (1985) 899–904.

[6] B. Mevel, J.L. Guyader, Routes to chaos in ball bearings, *Journal of Sound and Vibration* 162 (1993) 471–487.

[7] A. Sankaravelu, S.T. Noah, C.P. Burger, Bifurcation and chaos in ball bearings, *Nonlinear and Stochastic Dynamics* AMD-Vol. 192/ASME DE-Vol. 78 (1994) 313–325.

[8] H. Tamura, Y. Tsuda, On the static running accuracy of ball bearings, *Bulletin of the JSME* 28 (1985) 1240–1246.

[9] F.P. Gargiulo, A simple way to estimate bearing stiffness, *Machine Design* 52 (1980) 107–110.

[10] S. Yamauchi, The nonlinear vibration of flexible rotors, *Transactions of JSME* 446 (49) (1983) 1862–1868.

[11] S. Saito, Calculation of nonlinear unbalance response of horizontal Jeffcott rotors supported by ball bearings with radial clearances, *ASME Journal of Vibration Acoustics Stress and Reliability in Design* 107 (1985) 416–420.

[12] D.W. Childs, D.S. Moyer, Vibration characteristics of the high pressure oxygen turbopump of the space shuttle main engine, *Journal of Engineering for Gas Turbine and Power* 107 (1985) 152–159.

[13] Y.S. Choi, S.T. Noah, Nonlinear steady state response of a rotor support system, *ASME Journal of Vibration Acoustics Stress and Reliability in Design* 109 (1987) 255–261.

[14] C. Nataraj, H.D. Nelson, Periodic solutions in rotor dynamic systems with nonlinear supports; a general approach, *ASME Journal of Vibration Acoustics Stress and Reliability in Design* 111 (1989) 187–193.

[15] F.F. Ehrich, Subharmonic vibration of rotors in bearing clearance, *ASME-paper MD-I* 66 (1966) 281–289.

[16] F.F. Ehrich, Higher order subharmonic response of high speed rotors in bearing clearance, *ASME Journal of Vibration Acoustic Stress and Reliability in Design* 110 (1988) 9–16.

[17] F.F. Ehrich, Observation of subcritical superharmonic and chaotic response in rotor dynamic, *ASME Journal of Vibration Acoustic Stress and Reliability in Design* 114 (1991) 93–99.

[18] Y.B. Kim, S.T. Noah, Quasi-periodic response and stability analysis for a nonlinear Jeffcott rotor, *Journal of Sound and Vibration* 190 (2) (1996) 239–253.

[19] A. Choudhury, N. Tandon, A theoretical model to predict vibration response of rolling bearings to distributed defects under radial load, *ASME Journal of Vibration and Acoustics* 120 (1998) 214–220.
[20] L.D. Meyer, F.F. Ahlgran, B. Weichbrodt, An analytical model for ball bearing vibrations to predict vibration response to distributed defects, *ASME Journal of Mechanical Design* 102 (1980) 205–210.
[21] F.P. Wardle, S.Y. Poon, Rolling bearing noise, cause and cure, *Characterization in Mechanical Engineering* (1983) 36–40.
[22] F.P. Wardle, Vibration forces produced by waviness of the rolling surfaces of thrust loaded ball bearings—part I: theory, *Proceedings of the Institution of Mechanical Engineers* 202 (C5) (1988) 305–312.
[23] N. Aktürk, The effect of waviness on vibrations associated with ball bearings, *ASME Journal of Tribology* 121 (1999) 667–677.
[24] P. Eschmann, *Ball and Roller Bearings—Theory, Design and Application*, Wiley, New York, 1985.